Journal of Sound and Vibration 326 (2009) 599–622

Contents lists available at ScienceDirect

Journal of Sound and Vibration

journal homepage: www.elsevier.com/locate/jsvi

Lifting surface theory to predict aerodynamic forces induced by oscillating blades under interaction of three bladerows

Masanobu Namba *, Hiroyuki Nakagawa, Ayumi Kubo

Department of Aerospace Systems Engineering, Sojo University, 4-22-1 Ikeda, Kumamoto 860-0082, Japan

ARTICLE INFO

Article history:
Received 27 January 2009
Received in revised form
29 May 2009
Accepted 2 June 2009
Handling Editor: L.G. Tham
Available online 28 June 2009

ABSTRACT

The paper presents the unsteady lifting surface theory to predict unsteady aerodynamic forces on blades of aerodynamically coupled three annular bladerows. Blades of any one bladerow are assumed to be vibrating. The bladerows are assumed to be individually rotating with arbitrary rotational velocities, and therefore the model can be reduced to a rotor/stator/rotor model or a counter-rotating multi-rotor system model by appropriately specifying rotational velocity parameters. The details of the mathematical formulations and the solution procedures are described. Numerical studies were conducted. The disturbances produced by a simple harmonic blade vibration are composed of multiple frequency components because of aerodynamic interaction between bladerows in mutual rotational motions. Relative magnitudes of the frequency components of the unsteady aerodynamic forces are made clear. Not only the effects of nonoscillating neighboring bladerows on the unsteady aerodynamic response of the oscillating bladerow, but also the unsteady aerodynamic forces on nonoscillating neighboring bladerows induced by the oscillating bladerow are investigated.

1. Introduction

The key mechanism governing the classical two-degrees-of-freedom flutter of an airfoil is the modal coupling, i.e., the aerodynamic interaction between translational and pitching motions of the airfoil. The modal coupling is also the key factor governing a three-dimensional wing flutter. In this case more than three vibration modes are aerodynamically coupled.

As to the flutter of a bladerow composed of multiple blades, aerodynamic coupling among blades arises as an additional important factor. The importance of the interblade coupling is confirmed by the fact that the aerodynamic force on oscillating blades and the flutter boundary of a bladerow heavily depend on the interblade phase angle of blade vibration.

Directing the attention to actual multi-stage axial compressors and turbines, we have to further take into account the effect of interbladerow aerodynamic coupling. From recent studies based on models of multiple bladerows [1,2,4–9] it is now commonly understood that the unsteady aerodynamic response of oscillating blades is also significantly influenced by presence of neighboring bladerows in mutual motion.

The salient feature of the unsteady flow field in multi-stage bladerows is so-called frequency and mode scattering [10,11]. Unsteady disturbances originating from a simple harmonic oscillation of blades of one of the bladerows are scattered into multiple frequency components due to aerodynamic coupling between bladerows in mutual rotational

* Corresponding author. Tel./fax: +81 46 856 7028.
E-mail address: msnb-namba@jcom.home.ne.jp (M. Namba).

0022-460X/$ - see front matter © 2009 Elsevier Ltd. All rights reserved.
doi:10.1016/j.jsv.2009.06.002

Nomenclature

All quantities are made dimensionless with respect to
length r_T^* = tip radius
velocity W_a^* = mean axial flow velocity
density ρ_0^* = mean fluid density
pressure $\rho_0^* W_a^{*2}$
time r_T^*/W_a^*
Further the following notations are used:

$a(r,z)$ displacement amplitude of blade vibration normal to the blade surface
C_{aj} axial chord length of Row j
$C_{Lj(\alpha,\beta)}$ unsteady local lift coefficient of Row j of frequency $\omega_{j(\alpha,\beta)}$: Eq. (60)
CF_j generalized force on Row j: Eq. (65)
G_j axial coordinate position of the midchord section of Row j in the absolute cylindrical coordinate system
h hub-to-tip ratio
$\Im[\,]$ imaginary part of complex number
$\mathbf{K}_q$ velocity kernel function
M_a axial Mach number
N_{Bj} number of blades of Row j
n_j coordinate normal to (s_j, r) surface, i.e., constant η_j surface
$q_{0j}(r)$ $=\sqrt{1+\Omega_j^2 r^2}$: undisturbed flow velocity relative to Row j.
$\Re[\,]$ real part of complex number
Row 1 bladerow located at upstream station
Row 2 bladerow located at middle position
Row 3 bladerow located at downstream station
(r,θ,z) absolute (cylindrical) coordinate system fixed to the duct
(r,θ_j,z_j) coordinate system relatively fixed to Row j
s_j coordinate along an undisturbed streamline relative to Row j
t time
$\Delta p_j(r,z_j,t)$ unsteady pressure difference across a blade surface of Row j
$\eta_j=\theta_j-\Omega_j z_j$ helical coordinate
Ω_j rotational speed of Row j: $\Omega=\Omega^* r_T^*/W_a^*$.
ω reduced frequency $(\omega^* r_T^*/W_a^*)$ of the blade vibration
$\omega_{j(\alpha,\beta)}$ reduced frequency with integral mode parameters α and β in the frame of reference fixed to Row j: Eqs. (35), (37), (39)
σ interblade phase angle of bladerow vibration divided by blade-to-blade angle, i.e., number of nodal diameters of an annular bladerow vibration
$\sigma_{j(\alpha,\beta)}$ interblade phase angle divided by blade-to-blade angle of the duct mode related to the reduced frequency $\omega_{j(\alpha,\beta)}$ in the frame of reference fixed to Row j: Eqs. (36), (38), (40)
θ_{j0} angular position of the reference blade of Row j at time $t=0$ in the absolute coordinate system

Subscript

j row number ($j=1$, 2 or 3)
$j(\alpha,\beta)$ component of a fluctuating quantity with frequency $\omega_{j(\alpha,\beta)}$ in the frame of reference fixed to Row j
n_j component normal to a blade surface of Row j

motions. Therefore aerodynamic forces on all blades are composed of (infinite number of) multiple frequency components. Furthermore we should note that the frequency components are not independent but dependent on each other, even if small disturbance is assumed and the governing equations are linearized. Consequently when we deal with flutter problems of multi-stage bladerows, we encounter a heavy task of computing the unsteady flow fields and predicting the unsteady aerodynamic forces. In particular, the frequency and the mode of blade vibration at a critical flutter condition are essentially unknown values to be determined in the aeroelastic analysis, and it is necessary to conduct a lot of aerodynamic computations to search for the condition.

CFD techniques are now widely used to numerically simulate complicated unsteady flows in various problems. The techniques are categorized into two families: time-linearized frequency-domain solvers and nonlinear time-accurate time-domain solvers. The time-domain solvers provide straightforward time-marching simulations free from assumption of small disturbances. However, because of the very large computational times required, they are not suitable tools for the flutter analysis searching for the critical flutter conditions.

As far as problems of predicting critical flutter conditions are concerned, it is allowed to assume small unsteady disturbances. As mentioned above, however, the unsteady flows through multiple bladerows are composed of multiple frequency components dependent on each other, and therefore a simple harmonic time-dependence cannot be assumed. One of the solutions to cope with the problem in the category of time-linearized frequency-domain techniques is the harmonic balance technique developed by Hall et al. [3–6]. Those papers have provided new valuable knowledge as to the essential feature and magnitude of influence of neighboring bladerows on the aerodynamic response of an oscillating bladerow. However, although the harmonic balance technique is highly efficient compared with time-accurate solvers, the computational time required is not short enough to use as a tool of aerodynamic computation for the comprehensive aeroelastic flutter analysis.

The recent rapid progress in the electronic computer performance and the numerical computation technology has expelled the classical analytical methods from the leading role in the theoretical studies of fluid mechanics, because the applicability of the analytical methods is in general restricted to various assumptions, e.g., small disturbances, simple geometries, etc. Nevertheless because of the overwhelmingly high computation efficiency, they are still useful to conduct extensive studies on essential features of fundamental parameters.

The first author's research group has so far studied the problem of unsteady aerodynamics and flutter for a model of counter-rotating annular cascades by using an analytical method. The analytical method is an extension of the first author's unsteady linearized lifting surface theory for a rotating annular cascade to the model of a pair of counter-rotating cascades. A series of studies [7–9] have discovered the various aspects of the effect of a neighboring bladerow on the unsteady aerodynamic response of oscillating blades and the flutter condition.

The present paper gives an extension of the analytical method to a model of three bladerows, which can deal with the simultaneous influence of upstream and downstream bladerows. The same model has already been studied by Hall et al. on the bases of the two-dimensional cascade theory [2] and three-dimensional Euler equation solver for multistage bladerows [4]. The present paper aims at providing a more efficient calculation tool based on the linearized lifting surface theory, which enables one to conduct extensive aeroelastic analyses at a smaller computation cost. In fact, the present theory has recently been applied to the aeroelastic flutter analysis of the model of three bladerows, where the two rotor bladerows are simultaneously vibrating under aerodynamic coupling [12]. In that paper, however, the unsteady aerodynamic theory is only briefly described because of limited space.

This paper presents details of the unsteady lifting surface theory for a model of three bladerows formulated to calculate the unsteady loadings on blades which are caused by vibrations of blades in one of the three bladerows.

In this paper, moreover, numerical studies are also conducted to investigate the simultaneous effects of upstream and downstream neighboring bladerows on the aerodynamic response of oscillating blades. Furthermore, properties and magnitudes of unsteady aerodynamic forces not only on the vibrating blades themselves, but also on the stationary blades of the neighboring bladerows are investigated. In particular, the latter problem, i.e., how much aerodynamic forces are exerted on the neighboring bladerows, is of high interest, because it is directly associated with the possibility of interrow coupling flutter of multistage bladerows. However, this problem has been left unstudied.

2. Model description and mathematical formulation

2.1. Analytical model and geometries

We consider a model of three bladerows (Fig. 1) in an annular duct of an outer radius r_T^* and a hub-to-tip ratio h. The fluid is an inviscid nonconducting perfect gas. The undisturbed flow is of a subsonic uniform axial flow of a velocity W_a^*, a density ρ_0^* and an axial Mach number M_a. Hereafter unstarred symbols denote dimensionless quantities. Lengths, velocities, pressures, and times are normalized by r_T^*, W_a^*, $\rho_0 W_a^{*2}$, and r_T^*/W_a^*, respectively. We designate the bladerows by Row 1, Row 2 and Row 3, or by indices 1, 2 and 3. Row 1 is placed at the most upstream position, and is followed by Row 2 and Row 3 in the downstream direction. The mathematical formulations are made by assuming that the rows are rotating at individual angular velocities $\Omega_1 (= \Omega_1^* r_T^*/W_a^*)$, Ω_2 and Ω_3, for greater versatility in parameter selection. The model, however, reduces to a stator–rotor–stator model by specifying $\Omega_1 = \Omega_3 = 0$, and to a rotor–stator–rotor model by specifying $\Omega_2 = 0$. The signs of the rotational speeds are assumed as $\Omega_j > 0$ (clockwise looking from downstream) and $\Omega_j < 0$ (counterclockwise).

We denote cylindrical coordinate systems fixed to Row 1, Row 2, Row 3, and the duct by (r, θ_1, z_1), (r, θ_2, z_2), (r, θ_3, z_3), and (r, θ, z), respectively. The coordinates fixed to the duct and Row j are related with each other by

$$\theta = \theta_j - \Omega_j t + \theta_{j0}, \tag{1}$$

$$z = z_j + G_j, \tag{2}$$

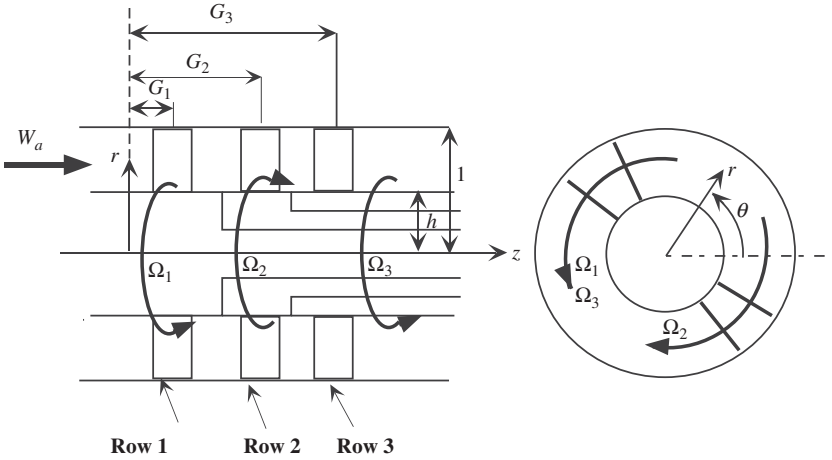

Fig. 1. Three bladerows in individual rotation.

where G_j denotes the axial position of the center of Row j in the duct-fixed coordinate system, and θ_{j0} denotes the angular position of the reference blade (numbered $m=0$) of Row j at time $t=0$. Further we define the helical coordinate η_j by

$$\eta_j = \theta_j - \Omega_j z_j. \tag{3}$$

The relationship of transformation between η_j with respect to Row j and $\eta_{j'}$ with respect to Row j' is given by

$$\eta_j = \theta_j - \Omega_j z_j = \theta + \Omega_j(t - z_j) - \theta_{j0} \tag{4}$$

$$= \eta_{j'} - (\Omega_{j'} - \Omega_j)(t - z_{j'}) + \Omega_j(G_j - G_{j'}) + \theta_{j'0} - \theta_{j0}. \tag{5}$$

Note that $\eta_j =$ constant corresponds to an undisturbed streamsurface in the frame of reference fixed to Row j.

We denote the numbers of blades of the bladerows by N_{B1}, N_{B2} and N_{B3}, and the axial chord lengths of the blades by C_{a1}, C_{a2} and C_{a3}. We assume that the blades are of constant axial chord length and no axial sweep and no dihedral lean.

2.2. Outline of mathematical formulation

Assume the blades of Row 1 are oscillating at an angular reduced frequency $\omega(=\omega^* r_T^*/W_a^*)$ and an inter-blade phase angle $2\pi\sigma/N_{B1}$, and further the blades of Row 2 and Row 3 are not vibrating. This assumption is just for the sake of brevity of expressions. The mathematical formulation can easily be made more comprehensive so that it can assume any one of the three bladerows is oscillating. The computation program developed in this study can deal with any case by specifying a row number of the vibrating bladerow.

Assume that the bladerows are operating with zero steady blade loading (zero time mean angle of attack, zero camber and zero thickness), and the amplitude of the blade oscillation is very small. Hence the flow field is governed by linearized equations.

Let the displacement normal to the blade surface of the m-th blade be given by

$$a(r,z)\mathrm{e}^{\mathrm{i}\omega t + \mathrm{i}2\pi m\sigma/N_{B1}} : m = 0, 1, \ldots, N_{B1} - 1. \tag{6}$$

Note that σ is an integral number corresponding to the number of nodal diameters of the annular bladerow vibration with a constant interblade phase angle. This blade motion generates a disturbance of time dependence and circumferential modes described as

$$D_1 = \mathrm{e}^{\mathrm{i}\omega t} \sum_{\mu_1=-\infty}^{\infty} D_{\mu_1}(r,z)\mathrm{e}^{\mathrm{i}(\mu_1 N_{B1}+\sigma)\theta_1}, \tag{7}$$

$$= \sum_{\mu_1=-\infty}^{\infty} D_{\mu_1}(r,z)\mathrm{e}^{\mathrm{i}\{\omega+(\mu_1 N_{B1}+\sigma)\Omega_1\}t + \mathrm{i}(\mu_1 N_{B1}+\sigma)(\theta-\theta_{10})}, \tag{8}$$

$$= \sum_{\mu_1=-\infty}^{\infty} D_{\mu_1}(r,z)\mathrm{e}^{\mathrm{i}\{\omega+(\mu_1 N_{B1}+\sigma)(\Omega_1-\Omega_2)\}t + \mathrm{i}(\mu_1 N_{B1}+\sigma)(\theta_2+\theta_{20}-\theta_{10})}, \tag{9}$$

$$= \sum_{\mu_1=-\infty}^{\infty} D_{\mu_1}(r,z)\mathrm{e}^{\mathrm{i}\{\omega+(\mu_1 N_{B1}+\sigma)(\Omega_1-\Omega_3)\}t + \mathrm{i}(\mu_1 N_{B1}+\sigma)(\theta_3+\theta_{30}-\theta_{10})}, \tag{10}$$

in terms of the frames of reference fixed to Row 1 (Eq. (7)), the duct (Eq. (8)), Row 2 (Eq. (9)), and Row 3 (Eq. (10)). Eqs. (9) and (10) imply that the disturbance D_1 is observed by Row 2 and Row 3 as a disturbance of multiple frequencies of $\omega + (\mu_1 N_{B1} + \sigma)(\Omega_1 - \Omega_2)$ and $\omega + (\mu_1 N_{B1} + \sigma)(\Omega_1 - \Omega_3)$, respectively.

Then interaction of the disturbance D_1 with Row 2 yields a new disturbance D_{1-2} described as

$$D_{1-2} = \sum_{\mu_1=-\infty}^{\infty} \mathrm{e}^{\mathrm{i}\{\omega+(\mu_1 N_{B1}+\sigma)(\Omega_1-\Omega_2)\}t} \sum_{\mu_2=-\infty}^{\infty} D_{\mu_1\mu_2}(r,z)\mathrm{e}^{\mathrm{i}\{\mu_2 N_{B2}+(\mu_1 N_{B1}+\sigma)\}\theta_2}, \tag{11}$$

$$= \sum_{\mu_1=-\infty}^{\infty}\sum_{\mu_2=-\infty}^{\infty} D_{\mu_1\mu_2}(r,z)\mathrm{e}^{\mathrm{i}\{\omega+(\mu_1 N_{B1}+\sigma)\Omega_1+\mu_2 N_{B2}\Omega_2\}t}\mathrm{e}^{\mathrm{i}\{\mu_2 N_{B2}+(\mu_1 N_{B1}+\sigma)\}(\theta-\theta_{20})}, \tag{12}$$

$$= \sum_{\mu_1=-\infty}^{\infty}\sum_{\mu_2=-\infty}^{\infty} D_{\mu_1\mu_2}(r,z)\mathrm{e}^{\mathrm{i}\{\omega+\mu_2 N_{B2}(\Omega_2-\Omega_1)\}t}\mathrm{e}^{\mathrm{i}\{\mu_2 N_{B2}+(\mu_1 N_{B1}+\sigma)\}(\theta_1+\theta_{10}-\theta_{20})}, \tag{13}$$

$$= \sum_{\mu_1=-\infty}^{\infty}\sum_{\mu_2=-\infty}^{\infty} D_{\mu_1\mu_2}(r,z)\mathrm{e}^{\mathrm{i}\{\omega+(\mu_1 N_{B1}+\sigma)(\Omega_1-\Omega_3)+\mu_2 N_{B2}(\Omega_2-\Omega_3)\}t}\mathrm{e}^{+\mathrm{i}\{\mu_2 N_{B2}+(\mu_1 N_{B1}+\sigma)\}(\theta_3+\theta_{30}-\theta_{20})}. \tag{14}$$

In the same manner, interaction of the disturbance D_1 with Row 3 gives rise to another disturbance D_{1-3} of a form similar to Eqs. (12)–(14). We should note that those disturbances D_{1-2} and D_{1-3} further interact with Row 3 and Row 2, respectively, and generate new disturbances D_{1-2-3}. It is easy to infer that the final form of the disturbance flow field is

expressed as

$$D_{1-2-3} = \sum_{\mu_1=-\infty}^{\infty}\sum_{\mu_2=-\infty}^{\infty}\sum_{\mu_3=-\infty}^{\infty} D_{\mu_1\mu_2\mu_3}(r,z)\mathrm{e}^{\mathrm{i}\omega_{\mu_1,\mu_2,\mu_3}t+\mathrm{i}n_{\mu_1,\mu_2,\mu_3}\theta}, \tag{15}$$

$$= \sum_{\mu_1=-\infty}^{\infty}\sum_{\mu_2=-\infty}^{\infty}\sum_{\mu_3=-\infty}^{\infty} D_{\mu_1\mu_2\mu_3}(r,z)\mathrm{e}^{\mathrm{i}\omega_{1(\mu_2,\mu_3)}t+\mathrm{i}(\mu_1 N_{B1}+\sigma_{1(\mu_2,\mu_3)})(\theta_1+\theta_{10})}, \tag{16}$$

$$= \sum_{\mu_2=-\infty}^{\infty}\sum_{\mu_3=-\infty}^{\infty}\sum_{\mu_1=-\infty}^{\infty} D_{\mu_1\mu_2\mu_3}(r,z)\mathrm{e}^{\mathrm{i}\omega_{2(\mu_3,\mu_1)}t+\mathrm{i}(\mu_2 N_{B2}+\sigma_{2(\mu_3,\mu_1)})(\theta_2+\theta_{20})}, \tag{17}$$

$$= \sum_{\mu_3=-\infty}^{\infty}\sum_{\mu_1=-\infty}^{\infty}\sum_{\mu_2=-\infty}^{\infty} D_{\mu_1\mu_2\mu_3}(r,z)\mathrm{e}^{\mathrm{i}\omega_{3(\mu_1,\mu_2)}t+\mathrm{i}(\mu_3 N_{B3}+\sigma_{3(\mu_1,\mu_2)})(\theta_3+\theta_{30})}, \tag{18}$$

where

$$\omega_{\mu_1,\mu_2,\mu_3} = \omega + (\mu_1 N_{B1} + \sigma)\Omega_1 + \mu_2 N_{B2}\Omega_2 + \mu_3 N_{B3}\Omega_3, \tag{19}$$

$$n_{\mu_1,\mu_2,\mu_3} = \sigma + \mu_1 N_{B1} + \mu_2 N_{B2} + \mu_3 N_{B3}, \tag{20}$$

$$\omega_{1(\mu_2,\mu_3)} = \omega + \mu_2 N_{B2}(\Omega_2 - \Omega_1) + \mu_3 N_{B3}(\Omega_3 - \Omega_1), \tag{21}$$

$$\sigma_{1(\mu_2,\mu_3)} = \sigma + \mu_2 N_{B2} + \mu_3 N_{B3}, \tag{22}$$

$$\omega_{2(\mu_3,\mu_1)} = \omega + \mu_3 N_{B3}(\Omega_3 - \Omega_2) + (\mu_1 N_{B1} + \sigma)(\Omega_1 - \Omega_2), \tag{23}$$

$$\sigma_{2(\mu_3,\mu_1)} = \sigma + \mu_3 N_{B3} + \mu_1 N_{B1}, \tag{24}$$

$$\omega_{3(\mu_1,\mu_2)} = \omega + (\mu_1 N_{B1} + \sigma)(\Omega_1 - \Omega_3) + \mu_2 N_{B2}(\Omega_2 - \Omega_3), \tag{25}$$

$$\sigma_{3(\mu_1,\mu_2)} = \sigma + \mu_1 N_{B1} + \mu_2 N_{B2}. \tag{26}$$

Note that Eq. (15) describes the flow field in terms of the frame of reference fixed to the duct, whereas Eqs. (16), (17) and (18) describe it in terms of the frames of reference fixed to Row 1, Row 2 and Row 3, respectively. Here, $\omega_{\mu_1,\mu_2,\mu_3}$ given by Eq. (19) denotes frequencies of the disturbance observed in the frame of reference fixed to the duct. The disturbance is composed of an infinite number of frequency components, which are identified by three integral parameters μ_1, μ_2 and μ_3. The fundamental frequency is the blade vibration frequency ω added by the nodal diameter passing frequency $\sigma\Omega_1$, where σ denotes the number of the nodal diameters of the blade vibration mode of Row 1. The frequencies other than the fundamental frequency are given by the fundamental frequency added by blade passing frequencies or their integral multiples of the three bladerows.

The space structure of the disturbance is constructed from spinning duct modes with circumferential wavenumbers n_{μ_1,μ_2,μ_3}, which are the nodal diameter σ added by positive or negative integral multiples of the numbers of blades of the three bladerows. Hereafter let us call the duct mode of $n_{0,0,0} = \sigma$ the fundamental duct mode, while the duct modes of $n_{\mu 1,\mu 2,\mu 3}$ with $\mu_1 \neq 0$ and/or $\mu_2 \neq 0$ and/or $\mu_2 \neq 0$ the derivative duct modes. Note that the wavenumbers of the derivative duct modes are not necessarily larger than the wavenumber of the fundamental duct mode. In the same way we call the component of the fundamental frequency $\omega_{j(0,0)}$ the fundamental frequency component, and the components of $\omega_{j(\alpha,\beta)}$ with $\alpha \neq 0$ and/or $\beta \neq 0$ the derivative frequency components.

We should note that the frequencies and the circumferential wavenumbers are identified by the same integral numbers μ_1, μ_2 and μ_3, but one frequency component does not necessarily correspond to one spinning mode. For instance, if Row 2 is not rotating ($\Omega_2 = 0$), no waves of the blade passing frequency and its multiples of Row 2 ($\mu_2 N_{B2}\Omega_2$) appear in the frame of reference fixed to the duct, but Row 2 still contributes to multiplication of duct modes via the terms $\mu_2 N_{B2}$ in Eq. (20).

On the other hand, Eqs. (21), (23) and (25) give frequencies of the disturbances observed in the frames of reference fixed to Row 1, Row 2 and Row 3, respectively, whereas Eqs. (22), (24) and (26) denote the interblade phase parameters of the disturbance components. For instance, the disturbance component with frequency $\omega_{1(\mu_2,\mu_3)}$ is observed in the frame of reference fixed to Row 1 with interblade phase angle $2\pi\sigma_{1(\mu_2,\mu_3)}/N_{B1}$. Note again that a co-rotating bladerow does not contribute to frequency multiplication, but still contributes to mode multiplication. For instance, if Row 1 and Row 3 are co-rotating ($\Omega_1 = \Omega_3$) and Row 1 is rotating relative to Row 2 ($\Omega_1 \neq \Omega_2$), the frequency $\omega_{1(\mu_2,\mu_3)}$ does not depend on the integral parameter μ_3 and depends on the parameter μ_2 alone, but the interblade phase parameter $\sigma_{1(\mu_2,\mu_3)}$ still depends on both μ_2 and μ_3.

Those expressions indicate that the unsteady blade loading of each row should be resolved into components identified by two integral parameters same as those in Eqs. (21)–(26). Let $\Delta p_j^{(m)}(r,z_j,t)$ denote the unsteady blade loading (lower surface pressure minus upper surface pressure) of the m-th blade of Row j. Then it can be expressed by

$$\Delta p_1^{(m)}(r,z_1,t) = \sum_{\mu_2=-\infty}^{\infty}\sum_{\mu_3=-\infty}^{\infty} \Delta p_{1(\mu_2,\mu_3)}(r,z_1)\mathrm{e}^{\mathrm{i}\omega_{1(\mu_2,\mu_3)}t+\mathrm{i}2\pi m\sigma_{1(\mu_2,\mu_3)}/N_{B1}}, \tag{27}$$

$$\Delta p_2^{(m)}(r,z_2,t)=\sum_{\mu_3=-\infty}^{\infty}\sum_{\mu_1=-\infty}^{\infty}\Delta p_{2(\mu_3,\mu_1)}(r,z_2)\mathrm{e}^{\mathrm{i}\omega_{2(\mu_3,\mu_1)}t+\mathrm{i}2\pi m\sigma_{2(\mu_3,\mu_1)}/N_{B2}},\tag{28}$$

$$\Delta p_3^{(m)}(r,z_3,t)=\sum_{\mu_1=-\infty}^{\infty}\sum_{\mu_2=-\infty}^{\infty}\Delta p_{3(\mu_1,\mu_2)}(r,z_3)\mathrm{e}^{\mathrm{i}\omega_{3(\mu_1,\mu_2)}t+\mathrm{i}2\pi m\sigma_{3(\mu_1,\mu_2)}/N_{B3}}.\tag{29}$$

The concept of the lifting surface theory is to regard those unsteady blade loadings as disturbance sources, and express the disturbance velocity field in the integral forms with kernel functions:

$$\begin{aligned}\mathbf{q}(r,\theta,z,t)=&\sum_{\mu_2=-\infty}^{\infty}\sum_{\mu_3=-\infty}^{\infty}\mathrm{e}^{\mathrm{i}\omega_{1(\mu_2,\mu_3)}t}\int_h^1\int_{-C_{a1}/2}^{C_{a1}/2}\Delta p_{1(\mu_2,\mu_3)}(\rho,\zeta)\\&\times\mathbf{K}_q(r,\eta_1,z_1-\zeta\,|\,\rho;N_{B1},\Omega_1,\omega_{1(\mu_2,\mu_3)},\sigma_{1(\mu_2,\mu_3)})\,\mathrm{d}\zeta\,\mathrm{d}\rho\\&+\sum_{\mu_3=-\infty}^{\infty}\sum_{\mu_1=-\infty}^{\infty}\mathrm{e}^{\mathrm{i}\omega_{2(\mu_3,\mu_1)}t}\int_h^1\int_{-C_{a2}/2}^{C_{a2}/2}\Delta p_{2(\mu_3,\mu_1)}(\rho,\zeta)\\&\times\mathbf{K}_q(r,\eta_2,z_2-\zeta\,|\,\rho;N_{B2},\Omega_2,\omega_{2(\mu_3,\mu_1)},\sigma_{2(\mu_3,\mu_1)})\,\mathrm{d}\zeta\,\mathrm{d}\rho\\&+\sum_{\mu_1=-\infty}^{\infty}\sum_{\mu_2=-\infty}^{\infty}\mathrm{e}^{\mathrm{i}\omega_{3(\mu_1,\mu_2)}t}\int_h^1\int_{-C_{a3}/2}^{C_{a3}/2}\Delta p_{3(\mu_1,\mu_2)}(\rho,\zeta)\\&\times\mathbf{K}_q(r,\eta_3,z_3-\zeta\,|\,\rho;N_{B3},\Omega_3,\omega_{3(\mu_1,\mu_2)},\sigma_{3(\mu_1,\mu_2)})\,\mathrm{d}\zeta\,\mathrm{d}\rho.\end{aligned}\tag{30}$$

Here $\mathbf{K}_q$ denotes the velocity kernel function. The details are given in Appendix A. Further noting that the kernel function is decomposed into circumferential wavenumber modes as

$$\mathbf{K}_q(r,\eta,z\,|\,\rho;N,\Omega,\omega,\sigma)=\sum_{\mu=-\infty}^{\infty}\mathrm{e}^{\mathrm{i}(\mu N+\sigma)\eta}\mathbf{K}_q^{(\mu)}(r,z\,|\,\rho;N,\Omega,\omega,\sigma),\tag{31}$$

we can rewrite Eq. (30) into

$$\begin{aligned}\mathbf{q}(r,\theta,z,t)=&\sum_{\mu_1=-\infty}^{\infty}\sum_{\mu_2=-\infty}^{\infty}\sum_{\mu_3=-\infty}^{\infty}\mathrm{e}^{\mathrm{i}\omega_{\mu_1,\mu_2,\mu_3}t+\mathrm{i}n_{\mu_1,\mu_2,\mu_3}\theta}\Bigg[\mathrm{e}^{-\mathrm{i}n_{\mu_1,\mu_2,\mu_3}(\Omega_1z_1+\theta_{10})}\int_h^1\int_{-C_{a1}/2}^{C_{a1}/2}\Delta p_{1(\mu_2,\mu_3)}(\rho,\zeta)\\&\times\mathbf{K}_q^{(\mu_1)}(r,z_1-\zeta\,|\,\rho;N_{B1},\Omega_1,\omega_{1(\mu_2,\mu_3)},\sigma_{1(\mu_2,\mu_3)})\,\mathrm{d}\zeta\,\mathrm{d}\rho\\&+\mathrm{e}^{-\mathrm{i}n_{\mu_1,\mu_2,\mu_3}(\Omega_2z_2+\theta_{20})}\int_h^1\int_{-C_{a2}/2}^{C_{a2}/2}\Delta p_{2(\mu_3,\mu_1)}(\rho,\zeta)\\&\times\mathbf{K}_q^{(\mu_2)}(r,z_2-\zeta\,|\,\rho;N_{B2},\Omega_2,\omega_{2(\mu_3,\mu_1)},\sigma_{2(\mu_3,\mu_1)})\,\mathrm{d}\zeta\,\mathrm{d}\rho\\&+\mathrm{e}^{-\mathrm{i}n_{\mu_1,\mu_2,\mu_3}(\Omega_3z_3+\theta_{30})}\int_h^1\int_{-C_{a3}/2}^{C_{a3}/2}\Delta p_{3(\mu_1,\mu_2)}(\rho,\zeta)\\&\times\mathbf{K}_q^{(\mu_3)}(r,z_3-\zeta\,|\,\rho;N_{B3},\Omega_3,\omega_{3(\mu_1,\mu_2)},\sigma_{3(\mu_1,\mu_2)})\,\mathrm{d}\zeta\,\mathrm{d}\rho\Bigg].\end{aligned}\tag{32}$$

So far we have assumed that the blades of Row 1 are vibrating. However, we can easily generalize the expressions for arbitrary cases. Let the row number of the bladerow with vibrating blades be j_ν. Then, we have just to rewrite Eqs. (19)–(26) into

$$\omega_{\mu_1,\mu_2,\mu_3}=\omega+\sigma\Omega_{j_\nu}+\mu_1N_{B1}\Omega_1+\mu_2N_{B2}\Omega_2+\mu_3N_{B3}\Omega_3,\tag{33}$$

$$n_{\mu_1,\mu_2,\mu_3}=\sigma+\mu_1N_{B1}+\mu_2N_{B2}+\mu_3N_{B3},\tag{34}$$

$$\omega_{1(\mu_2,\mu_3)}=\omega+\sigma(\Omega_{j_\nu}-\Omega_1)+\mu_2N_{B2}(\Omega_2-\Omega_1)+\mu_3N_{B3}(\Omega_3-\Omega_1),\tag{35}$$

$$\sigma_{1(\mu_2,\mu_3)}=\sigma+\mu_2N_{B2}+\mu_3N_{B3},\tag{36}$$

$$\omega_{2(\mu_3,\mu_1)}=\omega+\sigma(\Omega_{j_\nu}-\Omega_2)+\mu_3N_{B3}(\Omega_3-\Omega_2)+\mu_1N_{B1}(\Omega_1-\Omega_2),\tag{37}$$

$$\sigma_{2(\mu_3,\mu_1)}=\sigma+\mu_3N_{B3}+\mu_1N_{B1},\tag{38}$$

$$\omega_{3(\mu_1,\mu_2)}=\omega+\sigma(\Omega_{j_\nu}-\Omega_3)+\mu_1N_{B1}(\Omega_1-\Omega_3)+\mu_2N_{B2}(\Omega_2-\Omega_3),\tag{39}$$

$$\sigma_{3(\mu_1,\mu_2)}=\sigma+\mu_1N_{B1}+\mu_2N_{B2},\tag{40}$$

whereas, there is no need to rewrite expressions given by Eqs. (27)–(32).

3. Integral equations for blade loading functions

Eqs. (30) and (32) express the disturbance flow field as linearized superposition of disturbances generated from three bladerows. Here the unsteady blade loadings play roles of disturbance sources in appearance. We should recall, however, that the real origin of the disturbance is vibration of blades, and hence the unsteady blade loadings are not prescribable quantities but what should be calculated. The unsteady blade loadings are determined so that the disturbance velocity satisfies the flow tangency condition on blade surfaces.

Let the blades of Row j_ν be vibrating at a reduced frequency ω and an interblade phase angle $2\pi\sigma/N_{Bj_\nu}$ with normal displacement $a(r,z_{j_\nu})\mathrm{e}^{\mathrm{i}\omega t}$. Then, the flow tangency condition on the blade surfaces is expressed as follows:

$$[q_{nj}]_{\eta_j=\pm 0}=\delta_{jj_\nu}\left(\mathrm{i}\omega a(r,z_j)+\frac{\partial a(r,z_j)}{\partial z_j}\right)\mathrm{e}^{\mathrm{i}\omega t}:-C_{aj}/2\le z_j\le C_{aj}/2,\quad j=1,2,3. \tag{41}$$

Here q_{nj} denotes the n_j component of $\mathbf{q}$, i.e., the velocity component normal to blade surfaces of Row j. Further, δ_{jj_ν} denotes Kronecker delta. At a blade surface of Row j, it holds that $\eta_j=0$ and hence $\theta=-\Omega_j(t-z_j)+\theta_{j0}$. Then we have an expression as follows:

$$\begin{aligned}[q_{nj}]_{\eta_j=0}=&\sum_{\mu_1=-\infty}^{\infty}\sum_{\mu_2=-\infty}^{\infty}\sum_{\mu_3=-\infty}^{\infty}\mathrm{e}^{\mathrm{i}(\omega_{\mu_1,\mu_2,\mu_3}-n_{\mu_1,\mu_2,\mu_3}\Omega_j)t}\\
&\times\Bigg[\mathrm{e}^{-\mathrm{i}n_{\mu_1,\mu_2,\mu_3}\{(\Omega_1-\Omega_j)z_j-\Omega_1(G_1-G_j)+\theta_{10}-\theta_{j0}\}}\int_h^1\int_{-C_{a1}/2}^{C_{a1}/2}\Delta p_{1(\mu_2,\mu_3)}(\rho,\zeta)\\
&\times K^{(\mu_1)}_{qnj\leftarrow 1}(r,z_j-(G_1-G_j)-\zeta\,|\,\rho;N_{B1},\Omega_1,\omega_{1(\mu_2,\mu_3)},\sigma_{1(\mu_2,\mu_3)})\,\mathrm{d}\zeta\,\mathrm{d}\rho\\
&+\mathrm{e}^{-\mathrm{i}n_{\mu_1,\mu_2,\mu_3}\{(\Omega_2-\Omega_j)z_j-\Omega_2(G_2-G_j)+\theta_{20}-\theta_{j0}\}}\int_h^1\int_{-C_{a2}/2}^{C_{a2}/2}\Delta p_{2(\mu_3,\mu_1)}(\rho,\zeta)\\
&\times K^{(\mu_2)}_{qnj\leftarrow 2}(r,z_j-(G_2-G_j)-\zeta\,|\,\rho;N_{B2},\Omega_2,\omega_{2(\mu_3,\mu_1)},\sigma_{2(\mu_3,\mu_1)})\,\mathrm{d}\zeta\,\mathrm{d}\rho\\
&+\mathrm{e}^{-\mathrm{i}n_{\mu_1,\mu_2,\mu_3}\{(\Omega_3-\Omega_j)z_j-\Omega_3(G_3-G_j)+\theta_{30}-\theta_{j0}\}}\int_h^1\int_{-C_{a3}/2}^{C_{a3}/2}\Delta p_{3(\mu_1,\mu_2)}(\rho,\zeta)\\
&\times K^{(\mu_3)}_{qnj\leftarrow 3}(r,z_j-(G_3-G_j)-\zeta\,|\,\rho;N_{B3},\Omega_3,\omega_{3(\mu_1,\mu_2)},\sigma_{3(\mu_1,\mu_2)})\,\mathrm{d}\zeta\,\mathrm{d}\rho\Bigg].\end{aligned} \tag{42}$$

Here

$$\begin{aligned}K^{(\mu)}_{qnj\leftarrow j'}(r,z\,|\,\rho;N,\Omega,\omega,\sigma)=&\frac{1}{\sqrt{1+\Omega_{j'}^2r^2}\sqrt{1+\Omega_j^2r^2}}[-(\Omega_j-\Omega_{j'})K^{(\mu)}_{qs}(r,z\,|\,\rho;N,\Omega,\omega,\sigma)\\
&+(1+\Omega_j\Omega_{j'}r^2)K^{(\mu)}_{qn}(r,z\,|\,\rho;N,\Omega,\omega,\sigma)].\end{aligned} \tag{43}$$

It denotes the kernel function for the velocity component normal to the blades surfaces of Row j of the disturbances generated from the blade loadings of Row j'. Note that the expression of Eq. (42) is grouped by frequency, and it holds that

$$\omega_{\mu_1,\mu_2,\mu_3}-n_{\mu_1,\mu_2,\mu_3}\Omega_j=\left\{\begin{array}{l}\omega_{1(\mu_2,\mu_3)}:j=1\\ \omega_{2(\mu_3,\mu_1)}:j=2\\ \omega_{3(\mu_1,\mu_2)}:j=3\end{array}\right\}. \tag{44}$$

Then substituting Eq. (42) into Eq. (41) and requiring each frequency component to satisfy Eq. (41) individually, we obtain a system of integral equations for the unsteady blade loading functions as follows:

$$\begin{aligned}&\int_h^1\int_{-C_{a1}/2}^{C_{a1}/2}\Delta p_{1(\mu_2,\mu_3)}(\rho,\zeta)K_{qn}(r,0,z_1-\zeta\,|\,\rho;N_{B1},\Omega_1,\omega_{1(\mu_2,\mu_3)},\sigma_{1(\mu_2,\mu_3)})\,\mathrm{d}\zeta\,\mathrm{d}\rho\\
&+\sum_{\mu_1=-A}^{A}\mathrm{e}^{-\mathrm{i}n_{\mu_1,\mu_2,\mu_3}\{(\Omega_2-\Omega_1)z_1-\Omega_2(G_2-G_1)+\theta_{20}-\theta_{10}\}}\int_h^1\int_{-C_{a2}/2}^{C_{a2}/2}\Delta p_{2(\mu_3,\mu_1)}(\rho,\zeta)\\
&\times K^{(\mu_2)}_{qn1\leftarrow 2}(r,z_1-(G_2-G_1)-\zeta\,|\,\rho;N_{B2},\Omega_2,\omega_{2(\mu_3,\mu_1)},\sigma_{2(\mu_3,\mu_1)})\,\mathrm{d}\zeta\,\mathrm{d}\rho\\
&+\sum_{\mu_1=-A}^{A}\mathrm{e}^{-\mathrm{i}n_{\mu_1,\mu_2,\mu_3}\{(\Omega_3-\Omega_1)z_1-\Omega_3(G_3-G_1)+\theta_{30}-\theta_{10}\}}\int_h^1\int_{-C_{a3}/2}^{C_{a3}/2}\Delta p_{3(\mu_1,\mu_2)}(\rho,\zeta)\\
&\times K^{(\mu_3)}_{qn1\leftarrow 3}(r,z_1-(G_3-G_1)-\zeta\,|\,\rho;N_{B3},\Omega_3,\omega_{3(\mu_1,\mu_2)},\sigma_{3(\mu_1,\mu_2)})\,\mathrm{d}\zeta\,\mathrm{d}\rho\\
&=C_{1(\mu_2,\mu_3)}(r,z_1)\quad(\mu_2=0,\pm1,\ldots,\pm A;\ \mu_3=0,\pm1,\ldots,\pm A),\end{aligned} \tag{45}$$

$$\sum_{\mu_2=-A}^{A} \mathrm{e}^{-\mathrm{i}n_{\mu_1,\mu_2,\mu_3}\{(\Omega_1-\Omega_2)z_2-\Omega_1(G_1-G_2)+\theta_{10}-\theta_{20}\}} \int_h^1 \int_{-C_{a1}/2}^{C_{a1}/2} \Delta p_{1(\mu_2,\mu_3)}(\rho,\zeta)$$
$$\times K^{(\mu_1)}_{qn2\leftarrow 1}(r, z_2-(G_1-G_2)-\zeta\,|\,\rho;\, N_{B1}, \Omega_1, \omega_{1(\mu_2,\mu_3)}, \sigma_{1(\mu_2,\mu_3)})\,\mathrm{d}\zeta\,\mathrm{d}\rho$$
$$+ \int_h^1 \int_{-C_{a2}/2}^{C_{a2}/2} \Delta p_{2(\mu_3,\mu_1)}(\rho,\zeta) K_{qn}(r, 0, z_2-\zeta\,|\,\rho; N_{B2}, \Omega_2, \omega_{2(\mu_3,\mu_1)}, \sigma_{2(\mu_3,\mu_1)})\,\mathrm{d}\zeta\,\mathrm{d}\rho$$
$$+ \sum_{\mu_2=-A}^{A} \mathrm{e}^{-\mathrm{i}n_{\mu_1,\mu_2,\mu_3}\{(\Omega_3-\Omega_2)z_2-\Omega_3(G_3-G_2)+\theta_{30}-\theta_{20}\}} \int_h^1 \int_{-C_{a3}/2}^{C_{a3}/2} \Delta p_{3(\mu_1,\mu_2)}(\rho,\zeta)$$
$$\times K^{(\mu_3)}_{qn2\leftarrow 3}(r, z_2-(G_3-G_2)-\zeta\,|\,\rho; N_{B3}, \Omega_3, \omega_{3(\mu_1,\mu_2)}, \sigma_{3(\mu_1,\mu_2)})\,\mathrm{d}\zeta\,\mathrm{d}\rho$$
$$= C_{2(\mu_3,\mu_1)}(r, z_2) \quad (\mu_3 = 0, \pm 1, \ldots, \pm A;\ \mu_1 = 0, \pm 1, \ldots, \pm A), \tag{46}$$

$$\sum_{\mu_3=-A}^{A} \mathrm{e}^{-\mathrm{i}n_{\mu_1,\mu_2,\mu_3}\{(\Omega_1-\Omega_3)z_3-\Omega_1(G_1-G_3)+\theta_{10}-\theta_{30}\}} \int_h^1 \int_{-C_{a1}/2}^{C_{a1}/2} \Delta p_{1(\mu_2,\mu_3)}(\rho,\zeta)$$
$$\times K^{(\mu_1)}_{qn3\leftarrow 1}(r, z_3-(G_1-G_3)-\zeta\,|\,\rho;\, N_{B1}, \Omega_1, \omega_{1(\mu_2,\mu_3)}, \sigma_{1(\mu_2,\mu_3)})\,\mathrm{d}\zeta\,\mathrm{d}\rho$$
$$+ \sum_{\mu_3=-A}^{A} \mathrm{e}^{-\mathrm{i}n_{\mu_1,\mu_2,\mu_3}\{(\Omega_2-\Omega_3)z_3-\Omega_2(G_2-G_3)+\theta_{20}-\theta_{30}\}} \int_h^1 \int_{-C_{a2}/2}^{C_{a2}/2} \Delta p_{2(\mu_3,\mu_1)}(\rho,\zeta)$$
$$\times K^{(\mu_2)}_{qn3\leftarrow 2}(r, z_3-(G_2-G_3)-\zeta\,|\,\rho; N_{B2}, \Omega_2, \omega_{2(\mu_3,\mu_1)}, \sigma_{2(\mu_3,\mu_1)})\,\mathrm{d}\zeta\,\mathrm{d}\rho$$
$$+ \int_h^1 \int_{-C_{a3}/2}^{C_{a3}/2} \Delta p_{3(\mu_1,\mu_2)}(\rho,\zeta) K_{qn}(r, 0, z_3-\zeta\,|\,\rho; N_{B3}, \Omega_3, \omega_{3(\mu_1,\mu_2)}, \sigma_{3(\mu_1,\mu_2)})\,\mathrm{d}\zeta\,\mathrm{d}\rho$$
$$= C_{3(\mu_1,\mu_2)}(r, z_3) \quad (\mu_1 = 0, \pm 1, \ldots, \pm A;\ \mu_2 = 0, \pm 1, \ldots, \pm A), \tag{47}$$

where

$$C_{j(\alpha,\beta)}(r, z_j) = \delta_{j,j_v}\delta_{\alpha,0}\delta_{\beta,0}\left\{\mathrm{i}\omega a(r, z_j) + \frac{\partial}{\partial z_j} a(r, z_j)\right\}. \tag{48}$$

We should note that all blade loading components are dependent on each other, and cannot be determined individually. The numerical task to solve the system of integral equations must be carried out by truncating the infinite series to finite ones. As shown later, the most dominant components are the fundamental ones with integral mode parameters of zero, i.e., $\Delta p_{j(0,0)}(\rho,\zeta)$. Therefore, as shown in Eqs. (45)–(47), truncation should be made by retaining terms of the integral mode parameters from $-A$ to A, where A denotes an appropriate positive integral number. The previous studies on counter-rotating bladerows [7–9] indicate that computation even using A as small as $A = 1$ can give sufficiently good estimations of the fundamental frequency components $\Delta p_{j(0,0)}(r, z_j)$ from an engineering point of view.

4. Transform of integral equations into algebraic equations

Hereafter, all bladerows are assumed subsonic. Therefore relative flow velocity is subsonic at any radial station, i.e.,

$$M_a\sqrt{1+\Omega_j^2 r^2} < 1 \quad \text{for } h \le r \le 1, \tag{49}$$

for all three bladerows ($j = 1, 2$ and 3). Let the unsteady loading functions $\Delta p_{j(\alpha,\beta)}(\rho,\zeta)$ be expanded into mode function series as follows:

$$\Delta p_{j(\alpha,\beta)}(\rho,\zeta) = \sum_{k=0}^{L-1} R_k^{(\infty)}(\rho) \sum_{m=0}^{I-1} P_{j(\alpha,\beta)km} \Phi_m(\phi), \tag{50}$$

where

$$\Phi_0(\phi) = \cot(\phi/2), \quad \Phi_m(\phi) = \sin m\phi : (m \ge 1), \tag{51}$$

$$\zeta = -(C_{aj}/2)\cos\phi : 0 \le \phi \le \pi. \tag{52}$$

Further $R_k^{(\infty)}(\rho)$ is the radial eigenfunction of infinite circumferential order defined in Appendix B.2. The numbers of the finite series terms L and I should be selected from the accuracy point of view. The first author's previous studies on models of a single bladerow [13,14] assure that selection of $L = 7$ and $I = 7$ gives a sufficient accuracy from an engineering standpoint.

Substituting Eq. (50) into Eqs. (45)–(47), and formally conducting integrations with respect to ρ and ζ, we obtain algebraic equations for blade loading function coefficients $P_{j(\alpha,\beta)km}$ as follows:

$$\sum_{k=0}^{L-1}\sum_{m=0}^{I-1}\Bigg[P_{1(\mu_2,\mu_3)km}IK_{1\leftarrow 1(\mu_2,\mu_3)km}(r,z_1)+\sum_{\mu_1=-A}^{A}\{P_{2(\mu_3,\mu_1)km}IK^{(\mu_2)}_{1\leftarrow 2(\mu_3,\mu_1)km}(r,z_1-G_2+G_1) +P_{3(\mu_1,\mu_2)km}IK^{(\mu_3)}_{1\leftarrow 3(\mu_1,\mu_2)km}(r,z_1-G_3+G_1)\}\Bigg] = C_{1(\mu_2,\mu_3)}(r,z_1)\quad(\mu_2=0,\pm1,\ldots,\pm A;\ \mu_3=0,\pm1,\ldots,\pm A), \tag{53}$$

$$\sum_{k=0}^{L-1}\sum_{m=0}^{I-1}\Bigg[\sum_{\mu_2=-A}^{A}P_{1(\mu_2,\mu_3)km}IK^{(\mu_1)}_{2\leftarrow 1(\mu_2,\mu_3)km}(r,z_2-G_1+G_2) +P_{2(\mu_3,\mu_1)km}IK_{2\leftarrow 2(\mu_3,\mu_1)km}(r,z_2)+\sum_{\mu_2=-A}^{A}P_{3(\mu_1,\mu_2)km}IK^{(\mu_3)}_{2\leftarrow 3(\mu_1,\mu_2)km}(r,z_2-G_3+G_2)\Bigg] = C_{2(\mu_3,\mu_1)}(r,z_2)\quad(\mu_3=0,\pm1,\ldots,\pm A;\ \mu_1=0,\pm1,\ldots,\pm A), \tag{54}$$

$$\sum_{k=0}^{L-1}\sum_{m=0}^{I-1}\Bigg[\sum_{\mu_3=-A}^{A}\{P_{1(\mu_2,\mu_3)km}IK^{(\mu_1)}_{3\leftarrow 1(\mu_2,\mu_3)km}(r,z_3-G_1+G_3) +P_{2(\mu_3,\mu_1)km}IK^{(\mu_2)}_{3\leftarrow 2(\mu_3,\mu_1)km}(r,z_3-G_2+G_3)\}+P_{3(\mu_1,\mu_2)km}IK_{3\leftarrow 3(\mu_1,\mu_2)km}(r,z_3)\Bigg] = C_{3(\mu_1,\mu_2)}(r,z_3)\quad(\mu_1=0,\pm1,\ldots,\pm A;\ \mu_2=0,\pm1,\ldots,\pm A), \tag{55}$$

where

$$IK_{j\leftarrow j(\alpha,\beta)km}(r,z_j)=\int_h^1\int_0^\pi\frac{C_{aj}}{2}\sin\phi\,\Phi_m(\phi)R_k^{(\infty)}(\rho) \times K_{qn}(r,0,z_j+(C_{aj}/2)\cos\phi\mid\rho;N_{Bj},\Omega_j,\omega_{j(\alpha,\beta)},\sigma_{j(\alpha,\beta)})\,\mathrm{d}\rho\,\mathrm{d}\phi, \tag{56}$$

$$IK^{(\gamma)}_{j\leftarrow j'(\alpha,\beta)km}(r,z_j-G_{j'}+G_j) =\mathrm{e}^{-\mathrm{i}n_{\alpha,\beta,\gamma}\{(\Omega_{j'}-\Omega_j)z_j-\Omega_{j'}(G_{j'}-G_j)+\theta_{j'0}-\theta_{j0}\}}\int_h^1\int_0^\pi\frac{C_{aj'}}{2}\sin\phi\,\Phi_m(\phi)R_k^{(\infty)}(\rho) \times K^{(\gamma)}_{qnj\leftarrow j'}(r,z_j-G_{j'}+G_j+(C_{aj'}/2)\cos\phi\mid\rho;N_{Bj'},\Omega_{j'},\omega_{j'(\alpha,\beta)},\sigma_{j'(\alpha,\beta)})\,\mathrm{d}\rho\,\mathrm{d}\phi, \tag{57}$$

Note that the integrands of integrals with respect to ρ and ϕ in Eqs. (56) and (57) can be divided into two parts: a singular part that can analytically be integrated and a regular part that should numerically be integrated. But the accuracy of the numerical integration can be made as high as desired by increasing the numbers of integration points.

Letting Eqs. (53)–(55) be satisfied at L representative radial positions ($r=r_1,r_2,\ldots,r_L$) and I representative axial positions ($z_j=z_{j1},z_{j2},\ldots,z_{jI}$), we can determine the coefficients $P_{j(\alpha,\beta)km}$ as solutions of a system of linearized algebraic equations. The number of unknowns is equal to $L\times I\times(2A+1)^2\times 3$.

5. Unsteady aerodynamic characteristics

5.1. Unsteady aerodynamic force and moment

With regard to $a(r,z)$ in Eqs. (41) and (48), we can specify it by an appropriate mode shape function. We assume that $a(r,z)$ is a normalized function and the actual blade displacement is given by $A^*a(r,z)$. Note also that all aerodynamic force is composed of multiple frequencies $\omega_{j(\alpha,\beta)}$. Therefore all dimensionless aerodynamic parameters defined below are associated with the individual frequency components and expressed with a subscript $j(\alpha,\beta)$.

5.1.1. Unsteady pressure difference coefficient

The unsteady pressure difference across a blade surface is given by

$$\Delta p^*_{j(\alpha,\beta)}(\rho,\zeta)\mathrm{e}^{\mathrm{i}\omega_{j(\alpha,\beta)}t}=\mathrm{e}^{\mathrm{i}\omega_{j(\alpha,\beta)}t}(A^*/r_T^*)\rho_0^*W_a^{*2}\Delta p_{j(\alpha,\beta)}(\rho,\zeta), \tag{58}$$

where

$$\Delta p_{j(\alpha,\beta)}(\rho,\zeta)=\sum_{k=0}^{L-1}R_k^{(\infty)}(\rho)\sum_{m=0}^{I-1}P_{j(\alpha,\beta)km}\Phi_m(\phi). \tag{59}$$

5.1.2. Unsteady local lift coefficient

The unsteady local lift coefficient is defined by

$$C_{Lj(\alpha,\beta)}(r) \equiv \frac{\int_{-C_j^*/2}^{C_j^*/2} \Delta p^*_{j(\alpha,\beta)}\,\mathrm{d}s^*}{\rho_0^* W_a^{*2} C_j^* (A^*/r_T^*)}, \tag{60}$$

where $C_j^* = r_T^* C_{aj}\sqrt{1+\Omega_j^2 r^2}$ (local chord length) and $\mathrm{d}s^* = r_T^*\sqrt{1+\Omega_j^2 r^2}\,\mathrm{d}z$. Then

$$\begin{aligned} C_{Lj(\alpha,\beta)}(r) &= \frac{1}{C_{aj}}\int_{-C_{aj}/2}^{C_{aj}/2} \Delta p_{j(\alpha,\beta)}(r,z)\,\mathrm{d}z \\ &= \sum_{k=0}^{L-1} R_k^{(\infty)}(r)\, SP_{j(\alpha,\beta)k}, \end{aligned} \tag{61}$$

where

$$SP_{j(\alpha,\beta)k} = \frac{\pi}{2}\left(P_{j(\alpha,\beta)k0} + \frac{1}{2}P_{j(\alpha,\beta)k1}\right). \tag{62}$$

5.2. Generalized force

Let the blades of Row j be vibrating at a reduced frequency ω and a vibration mode $a(r,z_j)$. Then, the unsteady aerodynamic work on an vibrating blade per cycle is given by

$$W^* = \oint \mathrm{d}t r_T^* \int_h^1 \mathrm{d}r \int_{-C_j^*/2}^{C_j^*/2} \Re[\Delta p_j^*(r,z,t)]\Re\left[\frac{\mathrm{d}}{\mathrm{d}t}\{A^* a(r,z_j)\,\mathrm{e}^{\mathrm{i}\omega t}\}\right]\mathrm{d}s^* \tag{63}$$

$$= \rho_0^* W_a^{*2} r_T^{*3} (A^*/r_T^*)^2\,\pi \int_h^1 \sqrt{1+\Omega_j^2 r^2}\,\mathrm{d}r \int_{-C_{aj}/2}^{C_{aj}/2} \Im[\Delta p_{j(0,0)}(r,z_j)\overline{a(r,z_1)}]\,\mathrm{d}z_j. \tag{64}$$

Here $\overline{(\ )}$ denotes a complex conjugate.

As we have already seen, the unsteady blade loading is composed of various frequency components $\omega_{j(\alpha,\beta)} : \alpha = 0, \pm1, \pm2, \ldots, \pm A;\ \beta = 0, \pm1, \pm2, \ldots, \pm A$. But it is obvious that only the component of $\alpha = \beta = 0$ (the component of the blade vibration frequency; $\omega_{j(0,0)} = \omega$) acting on the vibrating blade itself contributes to the aerodynamic work per cycle. Noting that only blades of Row j are assumed to be vibrating, we define the dimensionless generalized force CF_j by

$$CF_j = \int_h^1 \sqrt{1+\Omega_j^2 r^2}\,\mathrm{d}r \int_{-C_{aj}/2}^{C_{aj}/2} \Delta p_{j(0,0)}(r,z_j)\overline{a(r,z_j)}\,\mathrm{d}z_j. \tag{65}$$

$$= \frac{C_{aj}}{2}\sum_{k=0}^{L-1}\sum_{m=0}^{l-1} P_{j(0,0)km} SAR_{j,km}, \tag{66}$$

where

$$SAR_{j,km} = \int_h^1 \sqrt{1+\Omega_j^2 r^2} R_k^{(\infty)}(r) \int_0^\pi \Phi_m(\theta)\overline{a(r,z)}\sin\theta\,\mathrm{d}\theta\,\mathrm{d}r. \tag{67}$$

The generalized force defined as above appears in flutter equations describing blade motions. In the present case the aerodynamic work per cycle on oscillating blade is given by

$$W^* = \rho_0^* W_a^{*2} r_T^{*3} \pi (A^*/r_T^*)^2\,\Im\left[CF_j\right]. \tag{68}$$

Therefore the stability or instability of the blade vibration can be identified by the sign of the imaginary part of the generalized force CF_j.

6. Numerical results and discussions

6.1. Specified conditions

We assume that the blade vibration is composed of the first-order bending mode and the first-order torsion mode, and the displacement amplitude normal to the blade surface is expressed by

$$a(r,z_j) = HC_{aj}h_1(r) + \Theta\theta_1(r)(z_j - z_e)\sqrt{1+\Omega_j^2 r^2}. \tag{69}$$

Here $H(=H^*/r_T^*)$ and Θ denote the translational displacement amplitude and the angle amplitude of bending and torsion, respectively, and z_e denotes the elastic axis position. Note that H and Θ are not necessarily real numbers. The mode shape functions $h_1(r)$ and $\theta_1(r)$ are assumed to be of uniform canti-lever beam and given by

$$h_1(r) = [(\sin \Upsilon_1 - \sinh \Upsilon_1)\{\sinh(\Upsilon_1 \Xi(r)) - \sin(\Upsilon_1 \Xi(r))\} + (\cosh \Upsilon_1 + \cos \Upsilon_1)\{\cosh(\Upsilon_1 \Xi(r)) - \cos(\Upsilon_1 \Xi(r))\}]/(2 \sin \Upsilon_1 \sinh \Upsilon_1) \quad (70)$$

and

$$\theta_1(r) = \sin(\pi \Xi(r)/2), \quad (71)$$

where $\Upsilon_1 = 0.597\pi$, $\Xi(r) = (r-h)/(1-h)$. Note that the mode functions are normalized so that $h_1(1) = 1$, $\theta_1(1) = 1$.

The conditions investigated in this paper are given in Table 1. Here we deal with combinations of stators and rotors. We denote the combinations by S1–R2–S3 and R1–S2–R3 instead of Row1–Row2–Row3. For comparison we also deal with combinations of two bladerows R1–S2, S1–R2 and so forth, and further an isolated bladerow S or R. The row of vibrating blades is not necessarily the middle one. We indicate it by (V), for instance, R1(V)–S2–R3. The relative Mach number for the rotor varies from 0.595 at the root to 0.9 at the tip, the stagger angle of the rotor varies from 40.89° at the root to 60° at the tip, and the pitch/chord ratio of the rotor varies from 0.396 at the root to 0.523 at the tip. On the other hand the pitch/chord ratio of the stator varies from 0.393 at the root to 0.7854 at the tip. Further in this paper, results are shown only for the blade vibration of the reduced frequency $\omega C_{aj} = 1.0$ and the bending vibration of $A^*/r_T^* = H \neq 0$, $\Theta = 0$.

The distances between two adjacent bladerows are assumed equal, i.e., $G_2 - G_1 = G_3 - G_2 = G$, and denoted by, e.g. $G = 1.2C_a$, where C_a is the mean axial chord length of the two adjacent bladerows.

6.2. Validation of computation programs, codes and term truncations

As to the numbers of the terms of the finite series expansion in Eq. (50), we took $L = 7$ and $I = 7$, which were found to give a sufficient accuracy in the previous studies [13,14]. To reconfirm the accuracy, we show the radial distributions of the fundamental frequency component of the local lift coefficient $C_{L2(0,0)}(r)$ on vibrating Rotor 2 computed using $L = 7$ and 9 in Fig. 2 and also the chordwise distributions of the fundamental frequency component of the pressure difference $\Delta p_{2(0,0)}(r,z)$ at midspan $r = 0.75$ computed using $I = 7$ and 11 in Fig. 3. Almost perfect coincidence is observed between $L = 7$ and 9. Difference between $I = 7$ and 11 is also very small.

On the other hand the integral numbers μ_1, μ_2, and μ_3 are truncated by specifying $A = 1$ in Eqs. (53)–(55), because the previous studies on counter-rotating bladerows indicated that $A = 1$ gives a sufficient accuracy for evaluation of the aerodynamic forces of the fundamental frequency component $\omega_j(0,0)$ as far as the relative flow velocities for all bladerows are subsonic. The effects of A in the present model are discussed later, too.

The computation procedure based on the present lifting surface theory is essentially straightforward. We have only to compute the coefficients $IK_{1\leftarrow 1(\mu_2,\mu_3)km\ell}(r,z_1)$, $IK^{(\mu_2)}_{1\leftarrow 2(\mu_3,\mu_1)km\ell}(r,z_1-G_2+G_1)$, etc. in Eqs. (53)–(55) and solve the linear algebraic system equations for $P_{1(\mu_2,\mu_3)km}$, etc. However, the mathematical expressions of the kernel functions are complicated, and hence the computation programs to compute the coefficients become highly complicated and lengthy. Therefore validation of the computation codes is required to assure the reliability of the numerical results.

The validity of the computation codes has already been proved in Ref. [12], where the result of the present theory is compared with the Euler code solution for a sample problem given in Ref. [4]. A good agreement between both solutions is shown in Fig. 2 of Ref. [12].

6.3. Frequency components of aerodynamic forces

The frequency spectrum of the aerodynamic forces on the blades and vanes is one of the matters of high interest. The frequency components of absolute values of the unsteady local lift coefficient $|C_{Lj(\alpha,\beta)}(r)|$ defined by Eq. (61) at midspan $r = 0.75$ are given in Figs. 4 and 5 for the cases of vibrating Rotor 2 at middle position (S1–R2(V)–S3) and vibrating Rotor 1 at upstream position (R1(V)–S2–R3), respectively. For comparison the values of an isolated rotor with a single frequency component are also shown.

Table 1
Specified parameters.

Hub/tip ratio h	0.5
Axial Mach number M_a	0.45
Number of rotor blades N_{Bj}	36
Number of stator vanes N_{Bj}	54
Axial chordlength (rotor) C_{aj}	6.0/36
Axial chordlength (stator) C_{aj}	8.0/54
Rotational speed (rotor) Ω_j	1.73205

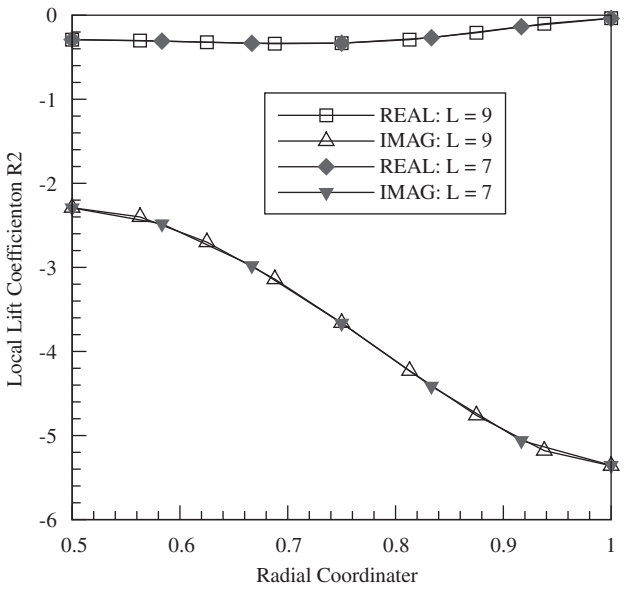

Fig. 2. The fundamental frequency component of the local lift coefficient $C_{L2(0,0)}(r)$ of vibrating Rotor 2. $\sigma = -10$. $G = 1.2C_a$. Comparison between computations with $L = 7$ and 9.

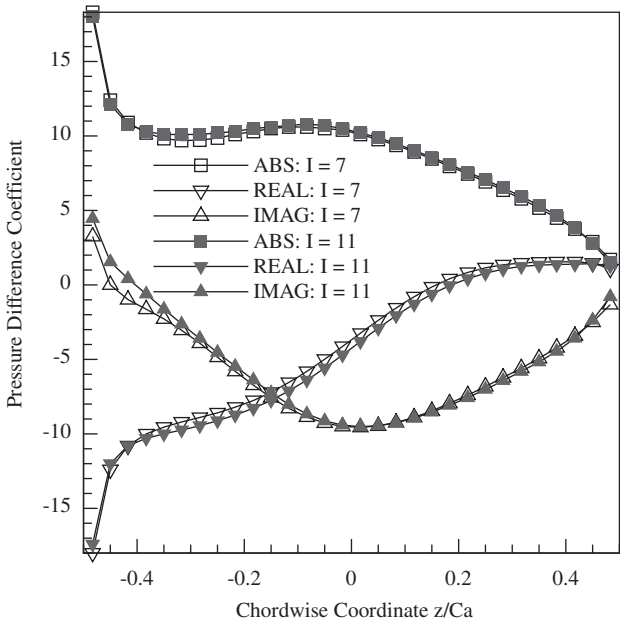

Fig. 3. The fundamental frequency component of the pressure difference $\Delta p_{(0,0)}(r,z)$ at midspan $r = 0.75$ of vibrating Rotor 2. $\sigma = -10$. $G = 1.2C_a$. Comparison between computations with $I = 7$ and 11.

Firstly, in general, the fundamental frequency component $(0,0)$, i.e., $(\alpha = 0, \beta = 0)$ is overwhelmingly dominant for each bladerow, and the derivative components ($\alpha \neq 0$ or $\beta \neq 0$) are very small.

Secondly, the aerodynamic force on the oscillating bladerow is larger than that on nonoscillating neighboring bladerows, but the latter is not very small.

Thirdly, as shown in Fig. 5, the vibrating upstream Rotor 1 gives a significant amount of aerodynamic force on co-rotating Rotor 3 located at the next to the next position. In other words, the influence of an oscillating bladerow on the next to the next bladerow is never small.

We should also note that the fundamental frequency of the aerodynamic force on Rotor 3 is equal to the frequency of blade vibration of Rotor 1. This fact was our motivation to conduct the analysis of interrow coupling flutter for the model of three bladerows in which two rotor bladerows are simultaneously vibrating [12].

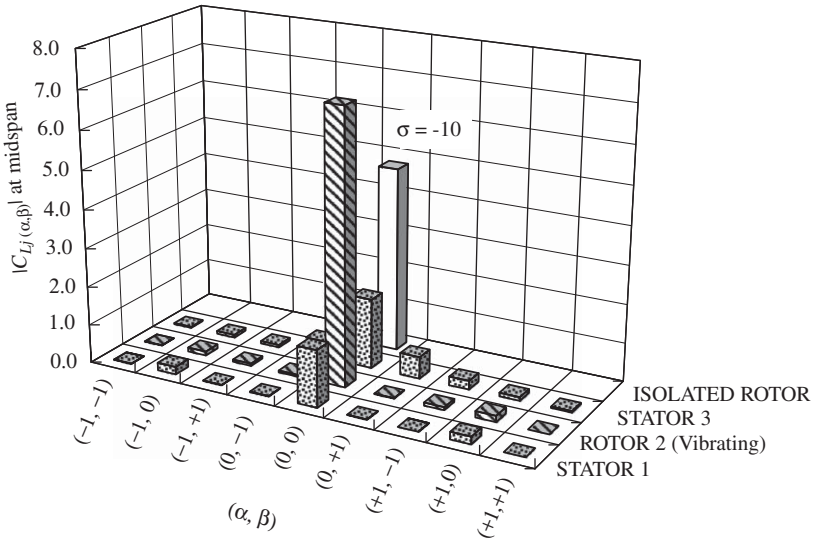

Fig. 4. The frequency components of the unsteady local lift coefficient $|C_{Lj(\alpha,\beta)}(r)|$ (absolute value) at midspan $r = 0.75$. $\sigma = -10$. Rotor 2 is vibrating ($j_v = 2$). $G = 1.2C_a$.

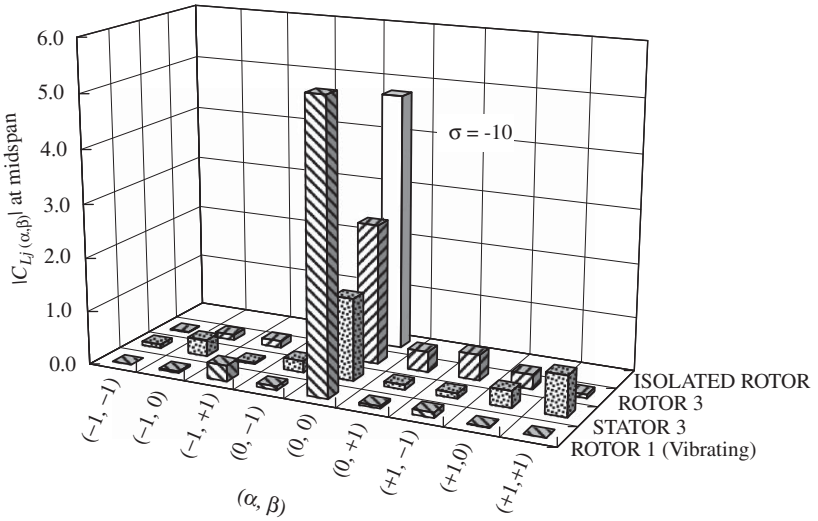

Fig. 5. The frequency components of the unsteady lift coefficient $|C_{Lj(\alpha,\beta)}(r)|$ (absolute value) at midspan $r = 0.75$. $\sigma = -10$. Rotor 1 is vibrating ($j_v = 1$). $G = 1.2C_a$.

6.4. *Effects of derivative duct modes on the fundamental force components*

As shown in Eq. (15), the disturbance flow field is composed of an infinite number of spinning duct modes. Note that the duct modes are identified by the circumferential wavenumber n_{μ_1,μ_2,μ_3} and the radial order (radial node number) ℓ. In our computation the radial node number is taken up to $\ell = L - 1 = 6$. Most dominant modes are the fundamental duct modes of the circumferential wavenumber $n_{0,0,0} = \sigma$, which are closely related to the fundamental components of the blade loadings $\Delta p_{1(0,0)}$, $\Delta p_{2(0,0)}$, and $\Delta p_{3(0,0)}$. On the other hand, the derivative duct modes with the circumferential wavenumbers of nonzero integral parameters (μ_1, μ_2, μ_3) are closely related to the derivative components of the blade loadings $\Delta p_{1(\mu_2,\mu_3)}$, $\Delta p_{2(\mu_3,\mu_1)}$, and $\Delta p_{3(\mu_1,\mu_3)}$. However we should note that the derivative duct modes also exert influence on the fundamental components of the blade loadings.

In order to see how much the fundamental components of the blade loadings are affected by the influence of the derivative duct modes, we compare in Fig. 6 the real part of the fundamental components of the unsteady local lift coefficients $C_{Lj(0,0)}(r)$ at midspan $r = 0.75$ obtained by computation using $A = 2$ and 1 , i.e., including the effects of the derivative duct modes to those obtained using $A = 0$, i.e., excluding derivative duct modes.

Firstly, as shown in the figures, the differences between the computations using $A = 1$ and 0 are remarkably small except at the interblade phase angles near $\pm\pi$ ($\sigma = \pm 18$), where minor differences are observed. This implies that the

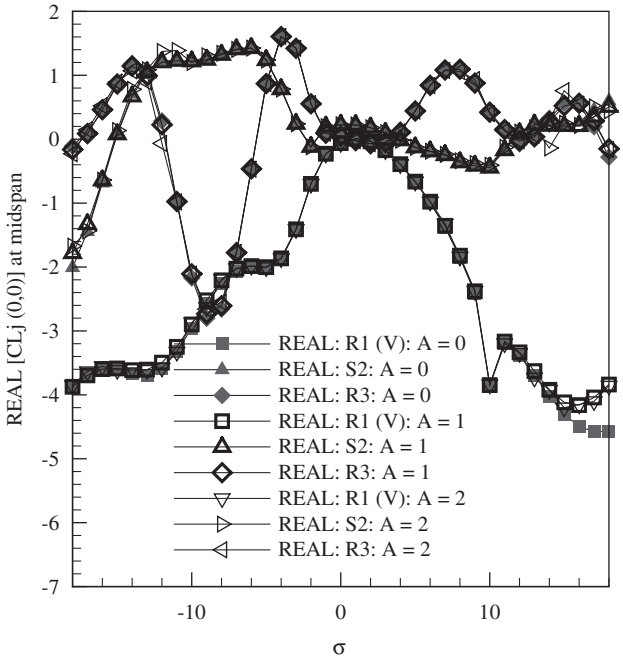

Fig. 6. Real part of the fundamental component of the unsteady local lift coefficient $C_{Lj(0,0)}(r)$ at midspan $r = 0.75$. Rotor 1 is vibrating ($j_\nu = 1$). $G = 1.2C_a$. Comparison between computations using $A = 2$, 1 and 0.

influence of the derivative duct modes on the fundamental components of the blade loadings is very small. The same knowledge has already been found in Ref. [4] for the fundamental component of the aerodynamic force on oscillating blades themselves $C_{L1(0,0)}$. The present results indicate that the minor influence of the derivative duct modes also holds true for the fundamental components of the aerodynamic forces on nonoscillating neighboring bladerows $C_{L2(0,0)}$ and $C_{L3(0,0)}$.

Secondly, no essential difference is observed between the computations using $A = 1$ and 2 even near $\sigma = \pm 18$. This suggests that selecting $A = 1$ is sufficient for predicting the fundamental frequency components of the aerodynamic forces.

We should note that the circumferential wavenumbers of the duct modes are given by $n_{\mu 1,\mu 2,\mu 3} = \sigma + (\mu_1 + \mu_2) \times 36 + \mu_2 \times 54$ for the example case. Then we can easily see that there are derivative duct modes with circumferential wavenumbers smaller than that of the fundamental duct mode, when σ is close to ± 18. The duct modes of small circumferential wavenumbers can be cut-on, and will contribute effectively to acoustic interbladerow interaction.

However, the fact that good estimations can be obtained using $A = 0$ for a wide range of the interblade phase angle is highly beneficial from the practical point of view, because computation costs, e.g., for flutter analyses, can drastically be reduced.

6.5. *Effects of neighboring blade rows on generalized forces*

Fig. 7 shows the generalized force on oscillating middle Rotor 2 (S1–R2(V)–S3) as a function of the interblade phase parameter σ. For comparison, the generalized forces for the combination of S1–R2(V) and the isolated rotor R(V) are also plotted. Here, we should note that the lowest order acoustic duct mode $(\sigma, 0)$, i.e., the circumferential wavenumber $n = \sigma$ and the radial order $\ell = 0$ is cut-on over the range $-1 < \sigma < 10$.

In this example, the row-to-row distance is small, i.e., $G = 1.2C_a$. Here C_a denote the average of axial chordlengths of the adjacent two bladerows. The difference from the values of the isolated bladerow for the case of S1–R(V)–S3 is significantly large and much higher than that for the case of S1–R(V). This indicates that the simultaneous reflecting effects of the adjacent upstream and downstream bladerows significantly modify the aerodynamic response of oscillating blades. We should also note that the influence is large in the range of cut-off of the duct mode $(\sigma, 0)$ rather than in the range of cut-on in this case of small bladerow gap.

In order to see the influence of the next to the next bladerow, we compare in Fig. 8 the case of R1(V)–S2–R3 with that of R1(V)–S2. The difference in the generalized force between the two cases is rather small. This suggests the reflecting effect of the next to the next bladerow on the aerodynamic response of oscillating blades is not significant. We should note, however, that it never means small aerodynamic influences of the oscillating blades on the next to the next bladerow, as is further discussed later.

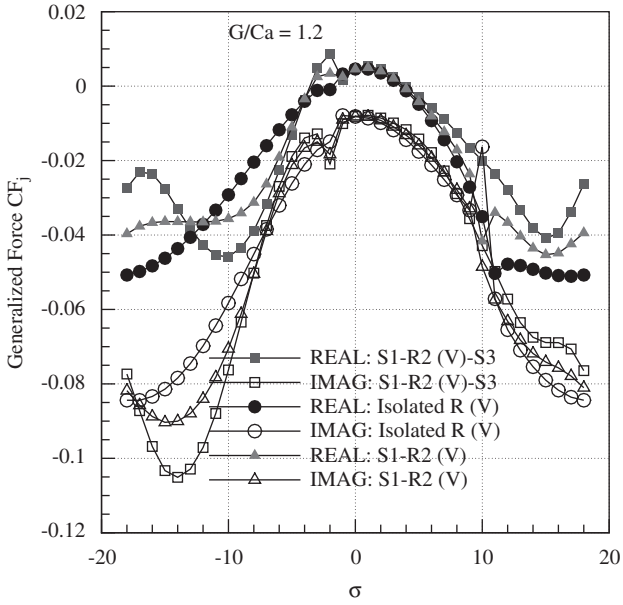

Fig. 7. The generalized force CF_j on vibrating Rotor 2. $G = 1.2C_a$.

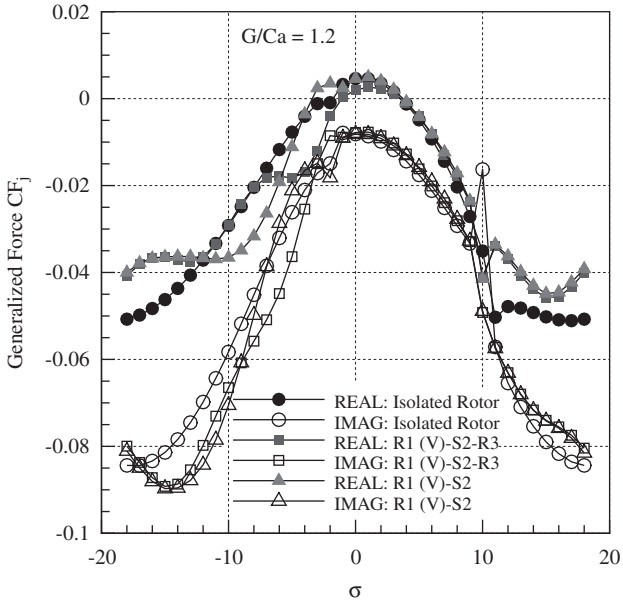

Fig. 8. The generalized force CF_j on vibrating Rotor 1. $G = 1.2C_a$.

The dependences of the neighboring bladerow effects on the bladerow gap are shown in Fig. 9. In the range where the duct mode $(\sigma, 0)$ is cut-off, the effects clearly become lower and lower as the bladerow gap increases. However, the effects do not become smaller in the cut-on range of the duct mode, i.e., $-1 < \sigma < 10$.

6.6. Induced aerodynamic forces on neighboring blade rows

In Fig. 10 the absolute values of the fundamental frequency component of the unsteady lift coefficient $|C_{Lj(0,0)}(r)|$ at midspan $r = 0.75$ on the oscillating bladerow and on the nonoscillating neighboring bladerows are plotted as functions of the interblade phase parameter σ for the case of S1–R2(V)–S3. It is seen again that the induced aerodynamic forces on the nonoscillating neighboring bladerows are not small. It is also observed that the influence on the downstream bladerow is mostly higher than that on the upstream bladerow.

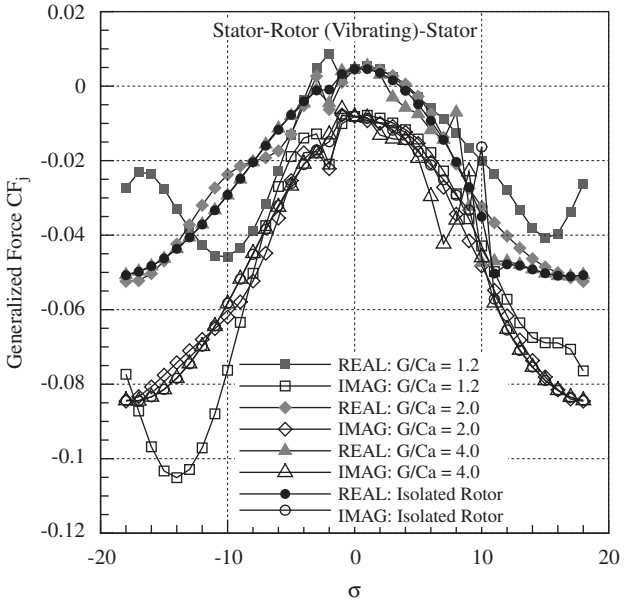

Fig. 9. The generalized force CF_j on vibrating Rotor 2. Dependence on the row-to-row distance G.

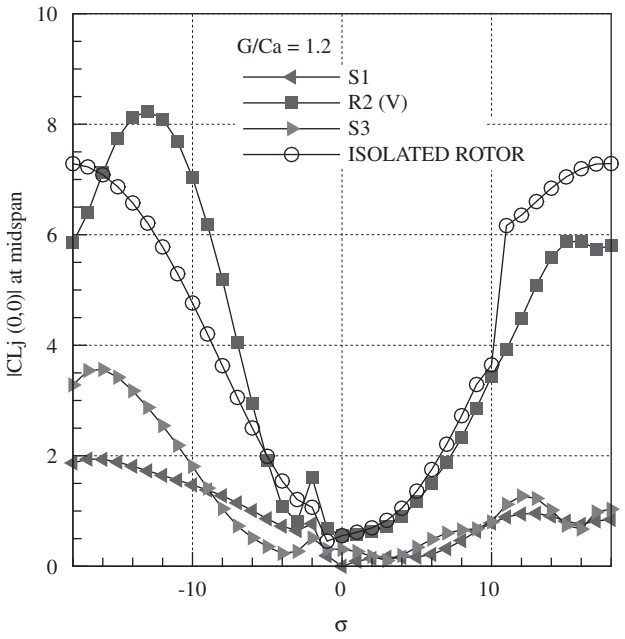

Fig. 10. The fundamental component of the local unsteady lift coefficient $|C_{Lj(0,0)}(r)|$ (absolute value) at midspan $r = 0.75$ on each bladerow. Rotor 2 is vibrating. $G = 1.2C_a$.

Fig. 11 shows the case of R1(V)–S2–R3. It should be noticed that the aerodynamic force induced on the next to the next bladerow is never small, and even larger than that on the next bladerow in a broad range of the interblade phase angle. Note again that the fundamental frequency of $C_{Lj(0,0)}$ of Rotor 3 is equal to the vibration frequency of Rotor 1. This suggests a strong possibility of aeroelastic mutual excitation of simultaneous vibration of the two rotors.

In Fig. 12 the cases of R1(V)–S2–R3 and R1–S2–R3(V) are compared. We can confirm that the influence on the next to the next bladerow at a downstream station is generally higher than that at an upstream station.

Fig. 13 shows the case of a wider bladerow gap ($G = 2.0C_a$). The difference in the aerodynamic force on oscillating bladerow between the case of R1(V)–S2–R3 and the isolated bladerow is clearly small. On the other hand, the aerodynamic

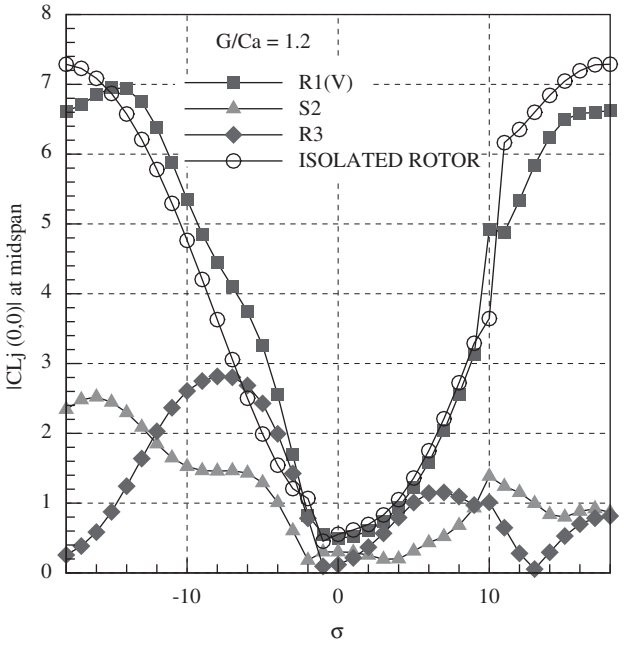

Fig. 11. The fundamental component of the local unsteady lift coefficient $|C_{Lj(0,0)}(r)|$ (absolute value) at midspan $r = 0.75$ on each bladerow. Rotor 1 is vibrating. $G = 1.2C_a$.

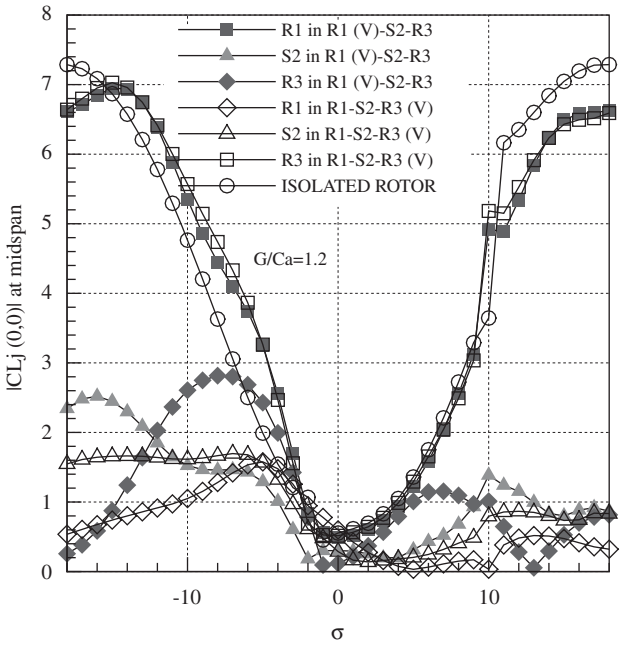

Fig. 12. The fundamental component of the local unsteady lift coefficient $|C_{Lj(0,0)}(r)|$ (absolute value) at midspan $r = 0.75$ on each bladerow. Comparison between vibrating Rotor 1 and vibrating Rotor 3. $G = 1.2C_a$.

force on the next to the next bladerow (Rotor 3) is certainly smaller than that of a smaller bladerow gap (Fig. 12). However, we should rather notice that it is not very small. It implies that the reflecting effect of the nonoscillating neighboring bladerows on the aerodynamic response of the oscillating bladerow becomes rapidly smaller as the bladerow gap increases, but the decrease in the induced aerodynamic forces on the nonoscillating neighboring bladerows with increase in the bladerow gap is rather slow.

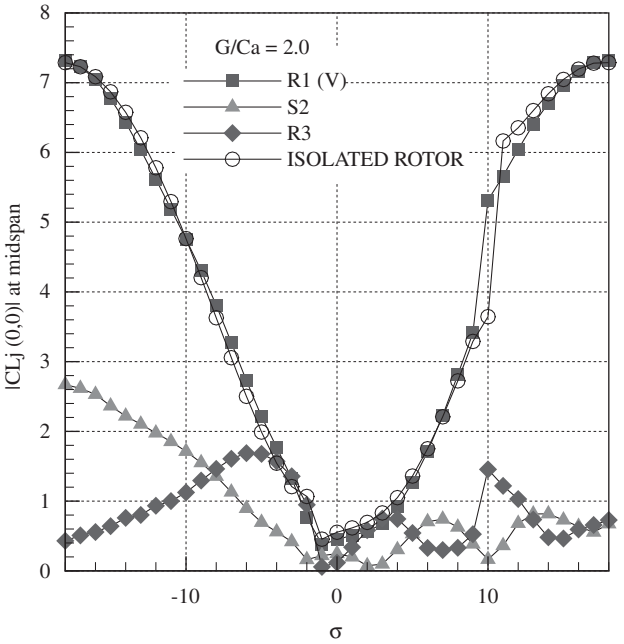

Fig. 13. The fundamental component of the local unsteady lift coefficient $|C_{Lj(0,0)}(r)|$ (absolute value) at midspan $r = 0.75$ on each bladerow. A wider bladerow gap $G = 2.0C_a$. Rotor 1 is vibrating.

7. Conclusions

The unsteady lifting surface theory for a model of three bladerows, blades of any one of the bladerows are oscillating, is developed. From numerical studies the following conclusions were drawn.

1. The fundamental frequency component of the unsteady aerodynamic force is overwhelmingly dominant not only for the oscillating bladerow but also for the nonoscillating neighboring bladerows.
2. The simultaneous reflecting effects of the adjacent upstream and downstream bladerows significantly modify the aerodynamic response of oscillating blades.
3. The reflecting effect of the next to the next bladerow on the aerodynamic response of oscillating blades is generally small.
4. In the cases of small bladerow gaps, the influence of the neighboring bladerows on the aerodynamic response of oscillating blades is higher outside the range where the lowest order acoustic duct mode is cut-on than inside the range.
5. The aerodynamic force induced by the oscillating bladerow is significant not only on the next bladerow but also on the next to the next bladerow.
6. The reflecting effect of the nonoscillating neighboring bladerows on the aerodynamic response of the oscillating bladerow becomes rapidly smaller as the bladerow gap increases, but the decrease in the induced aerodynamic forces on the nonoscillating neighboring bladerows with increase in the bladerow gap is rather slow.
7. The fundamental frequency components of the unsteady blade loadings are only slightly influenced by the presence of the derivative duct modes of the disturbances.

Appendix A. Kernel functions

A.1. Outline of kernel functions

Consider a rotor with the number of blades N rotating at an angular velocity Ω. Blades are straight with no sweep and lean, and the axial chord length C_a is constant along the span. Note that the blade chord length $C_a\sqrt{1+\Omega^2 r^2}$ is not constant. The time mean loading on blades are zero, i.e., the blades are twisted flat plates with zero mean angle of attack.

Assume that the blades are oscillating at an angular frequency ω and an interblade phase angle $2\pi\sigma/N$, where σ is an integral number between $-N/2$ and $N/2$. The integral number σ corresponds to the number of nordal diameter of the travelling wave mode of bladerow vibration. Then the blade oscillation causes an unsteady loading (fluctuating pressure

difference between the upper and lower surfaces), which can be described by $\Delta p(r,z)e^{i\omega t+i2\pi\sigma m/N}$: $(m=0,1,2,\ldots,N-1)$. Here m is a blade number.

Then the disturbance pressure p can be expressed in an integral form as follows:

$$p=\tilde{p}(r,\eta,z)e^{i\omega t}=e^{i\omega t}\int_h^1 d\rho\int_{-C_a/2}^{C_a/2}\Delta p(\rho,\zeta)K_p(r,\eta,z-\zeta|\rho;N,\Omega,\omega,\sigma)\,d\zeta. \tag{A.1}$$

Here K_p is the pressure kernel function given by

$$K_p(r,\eta,z-\zeta\,|\,\rho)=\left[\left(\frac{1}{\rho}\frac{\partial}{\partial\phi}-\Omega\rho\frac{\partial}{\partial\zeta}\right)G(r,\theta',z|\rho,\phi,\zeta)\right]_{\phi=\Omega\zeta,\theta'=\eta+\Omega z}, \tag{A.2}$$

and G is a Green function governed by

$$\left[\nabla^2-M_a^2\left(i\omega+\frac{\partial}{\partial z}+\Omega\frac{\partial}{\partial\theta'}\right)^2\right]G=\sum_{m=0}^{N-1}e^{i2\pi m\sigma/N}\frac{1}{r}\delta(r-\rho)\delta(\theta'-\phi-2\pi m/N)\delta(z-\zeta), \tag{A.3}$$

$$\frac{\partial G}{\partial r}=0\quad\text{at } r=1 \text{ and } h. \tag{A.4}$$

The disturbance velocity also can be expressed in an integral form:

$$\tilde{\mathbf{q}}(r,\eta,z)e^{i\omega t}=e^{i\omega t}\int_h^1 d\rho\int_{-C_a/2}^{C_a/2}\Delta p(\rho,\zeta)\mathbf{K}_q(r,\eta,z-\zeta|\rho;N,\Omega,\omega,\sigma)\,d\zeta, \tag{A.5}$$

where $\mathbf{K}_q$ is the velocity kernel function defined by

$$\mathbf{K}_q(r,\eta,z\,|\,\rho)=-e^{-i\omega z}\int_{-\infty}^{z}e^{i\omega z}[\nabla[K_p(r,\eta,z\,|\,\rho)]_{\eta=\theta'-\Omega z}]_{\theta'=\eta+\Omega z}\,dz. \tag{A.6}$$

A.2. Green function

Applying the standard method of solution to Eqs. (A.3) and (A.4), we obtain the following expression of the Green function:

$$G(r,\theta',z|\rho,\phi,\zeta)=-\frac{N}{4\pi\beta_a^2}\sum_{\mu_2=-\infty}^{\infty}\sum_{\ell=0}^{\infty}R_\ell^{(n)}(r)R_\ell^{(n)}(\rho)\frac{1}{\Lambda_\ell^{(n)}}E_\ell^{(n)}(\theta'-\phi,z-\zeta), \tag{A.7}$$

where

$$n=\nu N+\sigma,$$

$$E_\ell^{(n)}(\theta'-\phi,z-\zeta)=\exp[in(\theta'-\phi)+i(M_a^2/\beta_a^2)(\omega+n\Omega)(z-\zeta)-\Lambda_\ell^{(n)}|z-\zeta|], \tag{A.8}$$

$$\beta_a^2=1-M_a^2, \tag{A.9}$$

$$\Lambda_\ell^{(n)}=\left\{\begin{array}{c}\sqrt{D}:D>0\text{ cut-off mode}\\ i\,\mathrm{sgn}(\omega+\Omega n)\sqrt{-D}:D<0\text{ cut-on mode}\end{array}\right\}, \tag{A.10}$$

$$D=\frac{1}{\beta_a^2}\left((k_\ell^{(n)})^2-\frac{M_a^2}{\beta_a^2}(\omega+\Omega n)^2\right). \tag{A.11}$$

Further $R_\ell^{(n)}(r)$ and $k_\ell^{(n)}$ are the radial eigenfunction and the radial eigenvalue, respectively, which are explained in Appendix B. Further applying the finite series approximation described in Appendix B.2, we can rewrite the expression of the Green function as follows:

$$\begin{aligned}G(r,\theta',z\,|\,\rho,\phi,\zeta)=&-\frac{N}{4\pi\beta_a^2}\sum_{\nu=-\infty}^{\infty}\sum_{\ell=0}^{\infty}\sum_{j=0}^{L-1}\sum_{k=0}^{L-1}R_j^{(\infty)}(r)R_k^{(\infty)}(\rho)\\&\times BB_{\ell j}^{(n)}BB_{\ell k}^{(n)}\frac{1}{\Lambda_\ell^{(n)}}E_\ell^{(n)}(\theta'-\phi,z-\zeta),\end{aligned} \tag{A.12}$$

where $BB_{\ell k}^{(n)}$ is defined by Eq. (B.12) in Appendix B.2.

A.3. Expressions of the kernel functions

The pressure kernel function $K_p(r,\eta,z-\zeta\,|\,\rho)$ is obtained from differentiation of the Green function as shown by Eq. (A.2). Further, the velocity kernel function $\mathbf{K}_q(r,\eta,z-\zeta\,|\,\rho)$ is obtained from integration of differentiated pressure kernel function as shown by Eq. (A.6).

The velocity kernel function is expressed as a sum of circumferential mode components:

$$\mathbf{K}_q(r,\eta,z|\rho;N,\Omega,\omega,\sigma)=\sum_{v=-\infty}^{\infty}\mathrm{e}^{\mathrm{i}n\eta}\mathbf{K}_q^{(v)}(r,z|\rho;N,\Omega,\omega,\sigma)\quad(n=vN+\sigma). \tag{A.13}$$

The circumferential mode components of the normal-to-blade-surface velocity kernel function $K_{qn}^{(v)}$ and the streamwise velocity kernel function $K_{qs}^{(v)}$ are expressed as follows:

$$\begin{aligned}K_{qn}^{(v)}(r,z|\rho;N,\Omega,\omega,\sigma)=&\frac{\rho r}{q_0(r)}\frac{N}{4\pi\beta_a^2}\sum_{j=0}^{L-1}R_j^{(\infty)}(r)\sum_{k=0}^{L-1}R_k^{(\infty)}(\rho)\\&\times\sum_{\ell=0}^{L-1}\left\{\exp\left[\mathrm{i}\omega z\frac{M_a^2}{\beta_a^2}+\mathrm{i}n\Omega z\frac{1}{\beta_a^2}-\Lambda_\ell^{(n)}|z|\right]FN_{\ell jk}^{(n)}\right.\\&+\frac{1+\operatorname{sgn}z}{2}\mathrm{e}^{-\mathrm{i}\omega z}[(FN_{\ell jk(-)}^{(n)}-FN_{\ell jk(+)}^{(n)})\\&\left.-(FN_{\ell jk(-)}^{(\infty)}-FN_{\ell jk(+)}^{(\infty)})]\right\}:(n=vN+\sigma),\end{aligned} \tag{A.14}$$

$$\begin{aligned}K_{qs}^{(v)}(r,z|\rho;N,\Omega,\omega,\sigma)=&-\frac{1}{q_0(r)}\tilde{K}_p^{(v)}(r,z|\rho;N,\Omega,\omega,\sigma)\\&-\mathrm{i}\omega\frac{\rho}{q_0(r)}\frac{N}{4\pi\beta_a^2}\sum_{j=0}^{L-1}R_j^{(\infty)}(r)\sum_{k=0}^{L-1}R_k^{(\infty)}(\rho)\\&\times\sum_{\ell=0}^{L-1}\left\{\exp\left[\mathrm{i}\omega z\frac{M_a^2}{\beta_a^2}+\mathrm{i}n\Omega z\frac{1}{\beta_a^2}-\Lambda_\ell^{(n)}|z|\right]BB_{\ell j}^{(n)}BS_{\ell k}^{(n)}\right.\\&\left.+\frac{1+\operatorname{sgn}z}{2}\mathrm{e}^{-\mathrm{i}\omega z}BB_{\ell j}^{(n)}[BS_{\ell k(-)}^{(n)}-BS_{\ell k(+)}^{(n)}]\right\}:(n=vN+\sigma),\end{aligned} \tag{A.15}$$

$$FN_{\ell jk}^{(n)}=-DB_{\ell j}^{(n)}DB_{\ell k}^{(n)}\Lambda_\ell^{(n)}/DZ_\ell^{(n)}, \tag{A.16}$$

$$DZ_\ell^{(n)}=\mathrm{i}(n\Omega+\omega)/\beta_a^2-\Lambda_\ell^{(n)}\operatorname{sgn}(z-\zeta), \tag{A.17}$$

$$BS_{\ell k}^{(n)}=DB_{\ell k}^{(n)}/DZ_\ell^{(n)}, \tag{A.18}$$

$$DB_{\ell k}^{(n)}=\frac{\mathrm{i}}{\Lambda_\ell^{(n)}}\left\{BB_{\ell k}^{(n)}\Omega(n\Omega+\omega)\frac{M_a^2}{\beta_a^2}-n\,CB_{\ell k}^{(n)}\right\}-BB_{\ell k}^{(n)}\Omega\operatorname{sgn}(z-\zeta), \tag{A.19}$$

and $CB_{\ell k}^{(n)}$ is defined by Eq. (B.17) in Appendix B.2. Suffixes (+) and (−) denote values for $\operatorname{sgn}(z-\zeta)=+1$ and -1, respectively.

Appendix B. Radial eigenfunctions and radial eigenvalues

B.1. Strict solution

Eigenfunctions $R_\ell^{(n)}(r)$ and eigenvalues $k_\ell^{(n)}$ are defined by the following Sturm–Liouville boundary value problem:

$$\left[\frac{1}{r}\frac{\mathrm{d}}{\mathrm{d}r}\left(r\frac{\mathrm{d}}{\mathrm{d}r}\right)+\left((k_\ell^{(n)})^2-\frac{n^2}{r^2}\right)\right]R_\ell^{(n)}(r)=0, \tag{B.1}$$

$$\frac{\mathrm{d}}{\mathrm{d}r}R_\ell^{(n)}(r)=0\quad\text{at } r=1 \text{ and } h. \tag{B.2}$$

The eigenfunctions are orthogonal and normalized as follows:

$$\int_h^1 rR_m^{(n)}(r)R_\ell^{(n)}(r)\,\mathrm{d}r = \delta_{m\ell}. \tag{B.3}$$

Eq. (B.1) is the Bessel's differential equation, the general solution to which can be expressed as a linear combination of a Bessel function of the first kind and a Neuman's Bessel function of the second kind. We can determine the eigenvalues and eigenfunctions using the standard method of solving the Sturm–Liouville boundary value problem.

B.2. Finite series expansion of the radial eigenfunctions

The eigenfunctions $R_\ell^{(n)}(r)$ have no definite form for the circumferential wavenumber $n \to \infty$, and $R_\ell^{(n)}(r)$ for $n \to \infty$ can only be evaluated asymptotically [15]. Because of this character it is very difficult to separate the singular part from the Fourier–Bessel double series expressions of the kernel functions. To cope with the difficulty the technique of finite series expansion was invented by the first author [13,14]. The outline of the technique is described below.

The radial variation of the flow fields in axial turbomachines will be weak compared with the circumferential variation. Therefore the radial expansion series will be allowed to be truncated into a finite series expansion.

The finite series approximation consists of expressing $R_\ell^{(n)}(r)$ as a finite series in terms of 'base functions' $R_m^{(0)}(r)$, i.e., the zero-th-order eigenfunctions,

$$R_\ell^{(n)}(r) = \sum_{m=0}^{L-1} B_{\ell m}^{(n)} R_m^{(0)}(r), \tag{B.4}$$

and determine coefficients $B_{\ell m}^{(n)}$ so that Eq. (B.1) is satisfied in a weak form, i.e.,

$$\int_h^1 rR_k^{(0)}(r)\left[\frac{1}{r}\frac{\mathrm{d}}{\mathrm{d}r}\left(r\frac{\mathrm{d}}{\mathrm{d}r}\right) + \left((k_\ell^{(n)})^2 - \frac{n^2}{r^2}\right)\right]R_\ell^{(n)}(r)\,\mathrm{d}r = 0 \quad \text{for } k = 0, 1, \ldots, L-1, \tag{B.5}$$

which by use of the boundary condition, i.e., Eq. (B.2) becomes

$$\sum_{m=0}^{L-1} B_{\ell m}^{(n)}\left[\left((\kappa_\ell^{(n)})^2 - (k_m^{(0)}/n)^2\right)\delta_{mk} - R_{mk}\right] = 0 \quad \text{for } k = 0, 1, \ldots, L-1, \tag{B.6}$$

where

$$R_{mk} = \int_h^1 \frac{1}{r} R_m^{(0)}(r)R_k^{(0)}(r)\,\mathrm{d}r, \tag{B.7}$$

$$(\kappa_\ell^{(n)})^2 = (k_\ell^{(n)}/n)^2. \tag{B.8}$$

Eq. (B.6) implies that $(\kappa_\ell^{(n)})^2$ $(\ell = 0, 1, \ldots, L-1)$ and $B_{\ell m}^{(n)}$ $(\ell,\ m = 0, 1, \ldots, L-1)$ are eigenvalues and eigenvectors of a symmetric real matrix, the *mk* element of which is

$$R_{mk} + (k_m^{(0)}/n)^2\delta_{mk}. \tag{B.9}$$

One of the advantages of the finite series expansion is that one can define 'limit eigenfunctions' $R_\ell^{(\infty)}(r)$ and 'limit eigenvalues' $\kappa_\ell^{(\infty)}$. Letting $n \to \infty$ in Eq. (B.6), one can numerically determine $B_{\ell m}^{(\infty)}$ and $(\kappa_\ell^{(\infty)})^2$ as eigenvectors and eigenvalues of a matrix $[R_{\ell m}]$.

Then it holds that

$$R_m^{(0)}(r) = \sum_{\ell=0}^{L-1} B_{\ell m}^{(\infty)} R_\ell^{(\infty)}(r). \tag{B.10}$$

Substitution of Eq. (B.10) into Eq. (B.4) yields

$$R_\ell^{(n)}(r) = \sum_{k=0}^{L-1} BB_{\ell k}^{(n)} R_k^{(\infty)}(r), \tag{B.11}$$

where

$$BB_{\ell k}^{(n)} = \sum_{m=0}^{L-1} B_{\ell m}^{(n)} B_{km}^{(\infty)}. \tag{B.12}$$

Namely, $BB_{\ell k}^{(n)}$ are coefficients of a series for $R_\ell^{(n)}(r)$ expanded in terms of 'new base functions' $R_k^{(\infty)}(r)$.

The expansion of delta function $\delta(r-\rho)$ can be written as follows:

$$\delta(r-\rho)=\rho\sum_{m=0}^{L-1}R_m^{(n)}(r)R_m^{(n)}(\rho)=\rho\sum_{m=0}^{L-1}R_m^{(\infty)}(r)R_m^{(\infty)}(\rho). \tag{B.13}$$

Let $C_{\ell k}^{(n)}$ be coefficients of a series expansion of $(1/r^2)R_\ell^{(n)}(r)$ in terms of $R_m^{(0)}(r)$:

$$\frac{1}{r^2}R_\ell^{(n)}(r)=\sum_{m=0}^{L-1}C_{\ell m}^{(n)}R_m^{(0)}(r). \tag{B.14}$$

Then

$$C_{\ell m}^{(n)}=\int_h^1\frac{1}{r}R_m^{(0)}(r)R_\ell^{(n)}(r)\,\mathrm{d}r=\sum_{k=0}^{L-1}B_{\ell k}^{(n)}R_{mk}. \tag{B.15}$$

Substitution of Eq. (B.10) into Eq. (B.14) yields

$$\frac{1}{r^2}R_\ell^{(n)}(r)=\sum_{k=0}^{L-1}CB_{\ell k}^{(n)}R_k^{(\infty)}(r), \tag{B.16}$$

where

$$CB_{\ell k}^{(n)}=\sum_{m=0}^{L-1}C_{\ell m}^{(n)}B_{km}^{(\infty)}. \tag{B.17}$$

Namely $CB_{\ell k}^{(n)}$'s are coefficients of a series expansion of $(1/r^2)R_\ell^{(n)}(r)$ in terms of $R_k^{(\infty)}(r)$.

Appendix C. Expressions of coefficients of system equations

The functions $R_k^{(\infty)}(\rho)$, $\Phi_m(\phi)$ and $K_{qn}(r,0,z-\zeta|\rho)$ are known functions. Therefore the coefficient matrix $IK_{j\leftarrow j(\alpha,\beta)km}(r,z)$ defined by Eq. (56) can be obtained by conducting the integration. The expression of the integrand is too complicated to be integrated analytically, and the integration should be conducted numerically.

We should note, however, that the infinite series (A.13) is nonuniformly convergent series, and it is divergent at $z=0$ because $\lim_{n\to\infty}FN_{\ell jk}^{(n)}\neq 0$ in Eq. (A.14). In fact, the upwash velocity kernel function $K_{qn}(r,\eta,z-\zeta|\rho)$ is singular at an airfoil surface ($\eta=0, z=\zeta$) with singularities of $1/(z-\zeta)$ and $\log|z-\zeta|$. Therefore the Cauchy's principal value of integral must be calculated.

Numerical evaluation of the principal value of the integral should be avoided from the accuracy point of view. To attain high accuracy, we should separate the kernel function into a singular part and a regular part. The singular part can be expressed in terms of elementary functions, so that the principal value of the integral can be evaluated analytically. On the other hand the regular part is expressed in terms of uniformly convergent series, so that the numerical integration can be performed with a sufficient accuracy.

To extract the singular part from the nonuniformly convergent Fourier series, we should find the asymptotic behaviors of the terms at large wavenumbers.

In order to apply this method to the upwash velocity kernel function K_{qn} defined by Eqs. (A.13) and (A.14), we must make clear the asymptotic behaviors of $\Lambda_\ell^{(n)}$ defined by Eq. (A.10) and $FN_{\ell jk}^{(n)}$ defined by Eq. (A.16). After some laborious calculations, we can find

$$\Lambda_\ell^{(n)}=|n|\hat{\Lambda}_\ell^{(\infty)}-\frac{M_a^2}{\beta_a^4}\Omega\omega\frac{1}{\hat{\Lambda}_\ell^{(\infty)}}\operatorname{sgn}(n)+O(n^{-1}), \tag{C.1}$$

$$FN_{\ell jk}^{(n)}=FN_{\ell jk}^{(\infty)}+\delta_{\ell j}\delta_{\ell k}\frac{1}{|n|}\frac{\mathrm{i}\omega\kappa_\ell^{(\infty)2}}{\hat{\Lambda}_\ell^{(\infty)}}+O(n^{-2}), \tag{C.2}$$

at large n, where

$$FN_{\ell jk}^{(\infty)}=-\delta_{\ell j}\delta_{\ell k}\beta_a^2\hat{\Lambda}_\ell^{(\infty)}\{\operatorname{sgn}(z-\zeta)\beta_a^2\hat{\Lambda}_\ell^{(\infty)}-\mathrm{i}\operatorname{sgn}(n)\Omega\}, \tag{C.3}$$

$$\hat{\Lambda}_\ell^{(\infty)}=(1/\beta_a)\sqrt{\kappa_\ell^{(\infty)2}-(M_a^2/\beta_a^2)\Omega^2}, \tag{C.4}$$

$$\kappa_\ell^{(\infty)}=\lim_{n\to\infty}k_\ell^{(n)}/n. \tag{C.5}$$

We should like to emphasize that it is the method of the finite series expansion of the radial eigenfunctions described in Appendix B.2 that enables one to determine the definite values of $\kappa_\ell^{(\infty)}$ for individual radial order ℓ.

After some calculations, we finally obtains the following expressions:

$$IK_{j\leftarrow j(\alpha,\beta)km}(r,z_j)=\frac{C_{aj}}{2}\int_0^{\pi}TB_k(r,0,z_j+\frac{C_{aj}}{2}\cos\phi;j(\alpha,\beta))\Phi S_m(\phi)\,\mathrm{d}\phi$$
$$+\frac{\beta_a^2}{2}\frac{r}{\sqrt{1+\Omega_j^2r^2}}R_k^{(\infty)}(r)\hat{\Lambda}_{jk}^{(\infty)}\left\{\begin{array}{c}(-1):m=0\\ \cos m\theta:m\geq 1\end{array}\right\}$$
$$+\frac{\mathrm{i}}{4}\frac{r}{\sqrt{1+\Omega_j^2r^2}}R_k^{(\infty)}(r)\frac{\omega_{j(\alpha,\beta)}C_{aj}\kappa_k^{(\infty)2}}{\beta_a^2\hat{\Lambda}_{jk}^{(\infty)}}\left\{\begin{array}{c}(\log\frac{C_{aj}}{4}-\cos\theta):m=0\\ \frac{1}{2}(\log\frac{C_{aj}}{4}+\frac{1}{2}\cos 2\theta):m=1\\ \frac{1}{2}\left(\frac{\cos(m+1)\theta}{m+1}-\frac{\cos(m-1)\theta}{m-1}\right):m\geq 2\end{array}\right\},\tag{C.6}$$

$$\Phi S_m(\phi)=\left\{\begin{array}{c}1+\cos\phi:m=0\\ \sin m\phi\sin\phi:m\geq 1\end{array}\right\},\tag{C.7}$$

$$z_j=-(C_{aj}/2)\cos\theta,\tag{C.8}$$

$$TB_k(r,\eta,z;j(\alpha,\beta))=-\frac{N_{Bj}}{4\pi\beta_a^2}\frac{r}{\sqrt{1+\Omega_j^2r^2}}\left[\sum_{\nu=0}^{L-1}R_\nu^{(\infty)}(r)KQ_{\nu k}^{(R)}(z,\eta;\omega_{j(\alpha,\beta)},\sigma_{j(\alpha,\beta)})\right.$$
$$\left.+R_k^{(\infty)}(r)\{KQ_k^{(SW)}(z,\eta;\omega_{j(\alpha,\beta)},\sigma_{j(\alpha,\beta)})+KQ_k^{(SR)}(z,\eta;\omega_{j(\alpha,\beta)},\sigma_{j(\alpha,\beta)})\}\right].\tag{C.9}$$

Expressions of the functions $KQ_{\nu k}^{(R)}$, $KQ_k^{(SK)}$ and $KQ_k^{(SR)}$ are omitted to save space.

On the other hand, the bladerow coupling terms $IK_{j\leftarrow j'(\alpha,\beta)km}^{(\gamma)}(r,z_j-G_{j'}+G_j)$ defined by Eq. (56) have no singularity, and we can formally conduct integration with respect to ρ, and obtain the following expression:

$$IK_{j\leftarrow j'(\alpha,\beta)km}^{(\gamma)}(r,z_j-G_{j'}+G_j)$$
$$=\mathrm{e}^{-\mathrm{i}n_{\alpha,\beta,\gamma}\left\{(\Omega_{j'}-\Omega_j)z_j-\Omega_{j'}(G_{j'}-G_j)+\theta_{j'0}-\theta_{0j}\right\}}\frac{C_{aj'}}{2}\int_0^{\pi}\Phi S_m(\phi)$$
$$\times\left[K_{qnj\leftarrow j'}^{(\gamma,k)}(r,z_j-G_{j'}+G_j+\frac{C_{aj'}}{2}\cos\phi;N_{Bj'},\Omega_{j'},\omega_{j'(\alpha,\beta)},\sigma_{j'(\alpha,\beta)})\right]\mathrm{d}\phi,\tag{C.10}$$

where

$$\zeta=-(C_{aj}/2)\cos\phi,$$

$$K_{qnj\leftarrow j'}^{(\gamma,k)}(r,z;N_{Bj'},\Omega_{j'},\omega_{j'(\alpha,\beta)},\sigma_{j'(\alpha,\beta)})=\frac{1}{\sqrt{1+\Omega_{j'}^2r^2}\sqrt{1+\Omega_j^2r^2}}$$
$$\times\{-(\Omega_j-\Omega_{j'})rK_{qs}^{(\gamma,k)}(r,z;N_{Bj'},\Omega_{j'},\omega_{j'(\alpha,\beta)},\sigma_{j'(\alpha,\beta)})$$
$$+(1+\Omega_{j'}\Omega_jr^2)K_{qn}^{(\gamma,k)}(r,z;N_{Bj'},\Omega_{j'},\omega_{j'(\alpha,\beta)},\sigma_{j'(\alpha,\beta)})\},\tag{C.11}$$

$$K_{qn}^{(\gamma,k)}(r,z;N,\Omega,\omega,\sigma)=\frac{r}{\sqrt{1+\Omega^2r^2}}\frac{N}{4\pi\beta_a^2}\sum_{j=0}^{L-1}R_j^{(\infty)}(r)$$
$$\times\sum_{\ell=0}^{L-1}\left\{\exp\left[\mathrm{i}\omega z\frac{M_a^2}{\beta_a^2}+\mathrm{i}n\Omega z\frac{1}{\beta_a^2}-\Lambda_\ell^{(n)}|z|\right]FN_{\ell jk}^{(n)}\right.$$
$$\left.+\frac{1+\mathrm{sgn}\,z}{2}\mathrm{e}^{-\mathrm{i}\omega z}[(FN_{\ell jk(-)}^{(n)}-FN_{\ell jk(+)}^{(n)})-(FN_{\ell jk(-)}^{(\infty)}-FN_{\ell jk(+)}^{(\infty)})]\right\},\tag{C.12}$$

$$K_{qs}^{(\gamma,k)}(r,z;N,\Omega,\omega,\sigma)=\frac{1}{\sqrt{1+\Omega^2r^2}}\frac{N}{4\pi\beta_a^2}\sum_{j=0}^{L-1}R_j^{(\infty)}(r)\sum_{\ell=0}^{L-1}\exp\left[\mathrm{i}\omega z\frac{M_a^2}{\beta_a^2}+\mathrm{i}n\Omega z\frac{1}{\beta_a^2}-\Lambda_\ell^{(n)}|z|\right]BB_{\ell j}^{(n)}DB_{\ell k}^{(n)}$$
$$-\mathrm{i}\omega\frac{1}{\sqrt{1+\Omega^2r^2}}\frac{N}{4\pi\beta_a^2}\sum_{j=0}^{L-1}R_j^{(\infty)}(r)\sum_{\ell=0}^{L-1}\left\{\exp\left[\mathrm{i}\omega z\frac{M_a^2}{\beta_a^2}+in\Omega z\frac{1}{\beta_a^2}-\Lambda_\ell^{(n)}|z|\right]BB_{\ell j}^{(n)}BS_{\ell k}^{(n)}\right.$$
$$\left.+\frac{1+\operatorname{sgn}z}{2}\mathrm{e}^{-\mathrm{i}\omega z}BB_{\ell j}^{(n)}[BS_{\ell k(-)}^{(n)}-BS_{\ell k(+)}^{(n)}]\right\},\tag{C.13}$$

$$n=\gamma N+\sigma.\tag{C.14}$$

References

[1] K.K. Butenko, A.A. Osipov, Unsteady subsonic flow past two relatively moving flat cascades of thin weakly loaded oscillating blades, *Fluid Dynamics*, vol. 22, Plenum Publishing Corporation, New York, 1989, pp. 620–625 (0015-4628/88/2304-0620).

[2] K.C. Hall, P.D. Silkowski, The influence of neighboring blade rows on the unsteady aerodynamic response of cascades, *ASME Journal of Turbomachinery* 119 (1997) 85–93.

[3] K.C. Hall, J.P. Thomas, W.S. Clark, Computation of unsteady nonlinear flows in cascades using a harmonic balance technique, *AIAA Journal* 40 (5) (2002) 879–886.

[4] K.C. Hall, K. Ekici, D.M. Voytovych, Multistage coupling for unsteady flows in turbomachinery, *AIAA Journal* 43 (2005) 624–632.

[5] K. Ekici, D.M. Voytovych, K.C. Hall, Time-linearized Navier–Stokes analysis of flutter in multistage turbomachines, *43rd AIAA Aerospace Science Meeting and Exhibit*, Paper 2005-0836, Reno, NV, January 2005.

[6] K. Ekici, K.C. Hall, Nonlinear analysis of unsteady flows in multistage turbomachines using the harmonic balance technique, *44th AIAA Aerospace Science Meeting and Exhibit*, Paper 2006-0422, Reno, NV, January 2006.

[7] M. Namba, R. Nishino, Unsteady aerodynamic response of oscillating contra-rotating annular cascades, part I: description of model and mathematical formulations, *Transactions of the Japan Society for Aeronautical and Space Sciences* 49 (165) (2006) 175–180.

[8] R. Nishino, M. Namba, Unsteady aerodynamic response of oscillating contra-rotating annular cascades, part II: numerical study, *Transactions of the Japan Society for Aeronautical and Space Sciences* 49 (165) (2006) 181–186.

[9] M. Namba, R. Nishino, Flutter analysis of contra-rotating blade rows, *AIAA Journal* 44 (11) (2006) 2612–2620.

[10] D.A. Topol, Development and evaluation of a coupled fan noise design systems, AIAA Paper No. 97-1611, 1997.

[11] D.B. Hanson, Acoustic reflection and transmission of rotors and stators including mode and frequency scattering, AIAA Paper No. 97-1610-CP, 1997, pp. 199–210.

[12] M. Namba, A. Kubo, Aerodynamically coupled flutter of multiple blade rows, *Proceedings of ASME: Turbo & Expo 2008*, GT2008-50315, 2008.

[13] M. Namba, A. Ishikawa, Three-dimensional aerodynamic characteristics of oscillating supersonic and transonic cascades annular, *ASME Journal of Engineering for Power* 105 (1983) 138–146.

[14] M. Namba, Three-dimensional flows, in: M.F. Platzer, F.O. Carta (Eds.), *AGARD Manual on Aeroelasticity in Axial Flow Turbomachines*, Unsteady Turbomachinery Aerodynamics, vol. 1, AGARD-AG-298, Neuilly sur Seine, France, 1987.

[15] M. Abramowitz, I.A. Stegun, *Handbook of Mathematical Functions*, Dover Publications, New York, 1968, p. 365.